NONLINEAR DYNAMICS IN FLOW THROUGH UNSATURATED FRACTURED POROUS MEDIA: STATUS AND PERSPECTIVES

Boris Faybishenko
Earth Sciences Division
Ernest Orlando Lawrence Berkeley National Laboratory
Berkeley, California, USA

Received 21 January 2003; revised 1 January 2004; accepted 1 March 2004; published XX Month 2004.

[1] The need has long been recognized to improve predictions of flow and transport in partially saturated heterogeneous soils and fractured rock of the vadose zone for many practical applications, such as remediation of contaminated sites, nuclear waste disposal in geological formations, and climate predictions. Until recently, flow and transport processes in heterogeneous subsurface media with oscillating irregularities were assumed to be random and were not analyzed using methods of nonlinear dynamics. The goals of this paper are to review the theoretical concepts, present the results, and provide perspectives on investigations of flow and transport in unsaturated heterogeneous soils and fractured rock, using the methods of nonlinear dynamics and deterministic chaos. The results of laboratory and field investigations indicate that the nonlinear dynamics of flow and transport processes in unsaturated soils and fractured rocks arise from the dynamic feedback and competition between various nonlinear physical processes along with complex geometry of flow paths. Although direct measurements of variables characterizing the individual flow processes are not technically feasible, their cumulative effect can be characterized by analyzing time series data using the models and methods of nonlinear dynamics and chaos. Identifying flow through soil or rock as a nonlinear dynamical system is important for developing appropriate short- and long-time predictive models, evaluating prediction uncertainty, assessing the spatial distribution of flow characteristics from time series data, and improving chemical transport simulations. Inferring the nature of flow processes through the methods of nonlinear dynamics could become widely used in different areas of the earth sciences. *INDEX TERMS:* 5104 Physical Properties of Rocks: Fracture and flow; 3220 Mathematical Geophysics: Nonlinear dynamics; 1875 Hydrology: Unsaturated zone; 1832 Hydrology: Groundwater transport; *KEYWORDS:* nonlinear dynamics, chaos, unsaturated flow.

Citation: Faybishenko, B. (2004), Nonlinear dynamics in flow through unsaturated fractured porous media: Status and perspectives, *Rev. Geophys.*, *42*, XXXXXX, doi:10.1029/2003RG000125.

1. INTRODUCTION

[2] The intriguing word "chaos" has attracted the attention of many scientists and nonscientists for centuries. Hesiod was probably the first to introduce the word chaos in his *Theogony* (written in ~700 B.C.) as nothing but void, formless matter, infinite space. He appears to associate chaos with the great chasm, as some sort of gap between earth and sky; but chaos also represented the underworld or the earth. The first modern scientific application of the word chaos belongs to *Li and Yorke* [1975], who described the mathematical problem of a time evolution with sensitive dependence on initial conditions. Since the pioneering work of *Li and Yorke* [1975], chaos has been used in the scientific literature not only to define randomness but also to define the characteristics of chaotic dynamics generated by predominately deterministic processes. Chaotic dynamics, known popularly as chaos, is among the most fascinating new fields in modern science, reforming our perception of order and pattern in nature [*Gleick*, 1987]. Chaos theory has become a widely applied scientific concept, used in such larger constructs as "complexity theory" [*Nicolis and Prigogine*, 1989], "complex systems theory," "synergetics" [*Haken*, 1983], and "nonlinear dynamics" [*Abarbanel*, 1996]. Nonlinear dynamics is a fast developing field of physical sciences, with a wide variety of applications in such fields as biology [e.g., *May*, 1981; *Olsen et al.*, 1994], physics, chemistry, medicine, economics, earth sciences, and geology [e.g., *Hide*, 1994]. Chaotic dynamics is one of the fields within nonlinear dynamics. The term chaos theory is also used as a popular pseudonym for dynamic systems theory [*Abraham et al.*, 1997]. Note that chaos and turbulence (which were often used as synonyms in the scientific literature) represent two different types of processes [*Haken*, 1983].

[3] Some examples of dynamic systems that display nonlinear deterministic chaotic behavior with aperiodic and apparently random variability include atmospheric [*Lorenz*, 1963; *Nicolis*, 1987], geologic [*Turcotte*, 1997], geochemical [*Ortoleva*, 1994], and geophysical [*Dubois*,

1998; *Read*, 2001] processes, avalanches resulting from the perturbation of sandpiles of various sizes [*Rosendahl et al.*, 1993], falling of water droplets [*Cheng et al.*, 1989], river discharge and precipitation [*Pasternack*, 1999], oxygen isotope concentrations [*Nicolis and Prigogine*, 1989], viscous fingering in porous media [*Sililo and Tellam*, 2000], oscillatory fluid release during hydrofracturing in geopressured zones buried several kilometers in actively subsiding basins [*Dewers and Ortoleva*, 1994], thermal convection in porous media at large Rayleigh numbers [*Himasekhar and Bau*, 1986], and instabilities at fluid interfaces [*Moore et al.*, 2002]. It is noteworthy that experimental and theoretical investigations have shown that different physical, biological, mechanical, and chemical systems exhibit very similar (even universal) patterns, typical for deterministic chaotic systems. Nonetheless, up to now the practical application of chaos theory remains as much an art as a science.

[4] For many years the general approach to flow investigations in a fractured environment has been based on using stochastic methods to describe random-looking data sets [e.g., *Gelhar*, 1993], without considering that deterministic chaotic processes could cause apparent randomness of experimentally observed data.

[5] In his theoretical analysis of steady groundwater flow in a fully saturated, heterogeneous aquifer (with no discontinuities and a particular model for the spatial variability of hydraulic conductivity and based on Darcy's law), *Sposito* [1994] demonstrated the absence of chaos for groundwater flow as related to the impossibility of closed flow paths. The possibility of chaos is expected to occur in partially saturated, heterogeneous structured soils and fractured rock with discontinuity effects and drastic differences in permeability and flow mechanisms (such as those between high-conductivity flow channels and low-conductivity matrix).

[6] The goals of this paper are to review the theoretical concepts, present the results, and provide perspectives on investigations of flow and transport in unsaturated heterogeneous soils and fractured rock, using the methods of nonlinear dynamics and deterministic chaos. The paper is structured as follows: Section 2 presents a review of basic theoretical concepts and models of nonlinear dynamics. Section 3 provides an analysis of two key elements generating nonlinear dynamic and chaotic processes, geometry and physics of flow, and shows that unsaturated flow processes satisfy the criteria of a chaotic system. Section 4 provides some examples of chaos using pertinent results from laboratory and field infiltration experiments. Finally, section 5 gives concluding remarks and perspectives on using nonlinear dynamics in investigating unsaturated flow processes.

2. BACKGROUND OF NONLINEAR DYNAMICS AND CHAOS

2.1. Classification of Dynamic Systems and Definitions

2.1.1. Types of Dynamic Systems

[7] A dynamic system can be defined as a physical system with a time variation of system parameters. Dynamic systems are classified into two types: (1) deterministic (linear and nonlinear) and (2) stochastic. Deterministic systems are driven by a forcing function described explicitly to simulate the evolution of the system, implying that each state results in its unique consequence

$$Y_t = f(Y_{t-1}), \tag{1}$$

where Y_t is the value of the function at a time step t and Y_{t-1} is that at a previous time step $t - 1$; or a deterministic system may contain a random component that is not its driving force

$$Y_t = f(Y_{t-1}) + \varepsilon_t, \tag{2}$$

where ε_t is a random input (shock) function. Stochastic (or random) systems are driven by a random force described using a probabilistic function, e.g.,

$$Y_t = f(Y_{t-1}) + \pi_t, \tag{3}$$

where π_t is a random variable, being a driving force of the system at all times t. Time series data obtained from measurements of one of the system's variables can be used to infer whether the system is deterministic or stochastic or contains the properties of both of them.

[8] Dynamical systems are also classified as continuous and discrete systems. Continuous systems are characterized by the rate of change in their components, using a first-order differential equation, such as the basic growth/decay exponential law, implying that the rate of change for a system parameter x is proportional to its value

$$d/dt\, x(t) = \alpha x(t), \tag{4}$$

where $\alpha > 0$ is a growth constant and $\alpha < 0$ is a decay constant. The solution of equation (4) is $x(t) = e^{\alpha t} x_o$. Discrete systems are characterized by a series of events with discrete time intervals, described by difference equations, such as the basic growth/decay law stating that the relationship between the value x at a time $\tau + 1$ is proportional to its value at the time τ

$$x_{\tau+1} = \alpha x_\tau. \tag{5}$$

A dynamic system described by a set of differential equations with continuous solutions is called a flow, and a system described by a set of difference equations is called a map [*Tsonis*, 1992].

[9] The term deterministic chaos is used to describe a dynamic process with random-looking, erratic data, in which the variable $x(t)$ undulates nonperiodically and never settles on a constant value and random processes are not a dominant part of the system [*Moon*, 1987; *Schuster*, 1988; *Tsonis*, 1992]. Although chaotic fluctuations can be described by nonlinear ordinary or partial differential equations, which could theoretically be purely deterministic, with no random quantities, real physical processes usually contain a stochastic (or noise) component [*Haken*, 1983; *Kapitaniak*, 1988; *Yao and Tong*, 1994]. A stochastic

chaotic system is a system in which both deterministic and stochastic processes play a significant role in system dynamics. A combination of deterministic and stochastic processes may result in a system in which deterministic (nonchaotic) processes are interrupted with irregular shocks [*Schuster*, 1988]. It is important to discriminate whether an irregular behavior is caused by nonlinear deterministic chaotic dynamics or by nonlinear stochastic dynamics [*Timmer et al.*, 2000].

2.1.2. Criteria of a Deterministic Chaotic System

[10] The physical system may exhibit a deterministic chaotic behavior under the following conditions:

[11] 1. The system is dissipative, which, unlike a conservative system, is (1) an open system, exchanging energy, matter, and information with the surrounding environment [*Prigogine and Stengers*, 1997], and (2) characterized by the presence of irreversible processes, disequilibrium, and self-organization, e.g., the ability to organize or arrange the system's behavior [*Nicolis and Prigogine*, 1989]. Examples of dissipative systems are electrical circuits, in which some electric and magnetic energy is dissipated in the resistors as the heat, or viscoelastic mechanical systems with friction that causes a loss of energy. One of the essential properties of a dissipative system is fluctuation of system microcomponents [*Haken*, 1983; *Nicolis and Prigogine*, 1989], which is often observed in physical, chemical, and biological systems near a critical state, i.e., where the system can change its macroscopic state. (Note that dissipative systems may exhibit monotonic behavior because of volume and time averaging of variables measured to characterize the system.)

[12] 2. The system is nonlinear; coupled effects of several nonlinear processes are governed by nonlinear ordinary or partial differential equations with bounded nonperiodic solutions.

[13] 3. The system behavior is sensitive to small variations in initial conditions. For example, Figure 1 demonstrates the paths of seven sliding boards down a slope, starting with identical velocities from points spaced at 1-mm intervals. Figure 1 demonstrates that in a chaotic system, nearby states will eventually diverge no matter how small the initial difference is [*Lorenz*, 1997]. Such a system essentially forgets its initial conditions and cannot exactly repeat its past behavior, so that the information on initial conditions cannot be recovered from later states of the system.

[14] 4. Intrinsic properties of the system, not random external factors, cause an irregular, chaotic dynamic for system components. In a deterministic chaotic system, new emergent structures and properties may arise without being affected by externally imposed boundary conditions.

[15] Note that the presence of nonlinearity [*Acheson*, 1997] and dissipation [*Tsonis*, 1992] are insufficient for a system to be chaotic.

2.1.3. Routes to Chaos

[16] Using the analysis of the phase space trajectories, several types of routes to chaos can be identified: bifurcations (period doubling, pitchfork, subtle, catastrophic, explosive, symmetric, or asymmetric), intermittency, and collapse of quasiperiodicity [*Tsonis*, 1992; *Arnold*, 1984]. Figure 2 demonstrates two types of an intermittency route to chaos. Figure 2a gives an example of a signal alternating in time between long regular (e.g., laminar) phases and relatively short irregular (e.g., random or deterministic chaotic) bursts, indicating that the system exhibits a discontinuous dynamics over time [*Schuster*, 1988]. Figure 2b presents an example of quasiperiodic behavior (shown as phase 1 in Figure 2b), alternating with another type (phase 2) of quasiperiodicity [*Rabinovich and Trubetskov*, 1994] (an example is demonstrated in section 4.2).

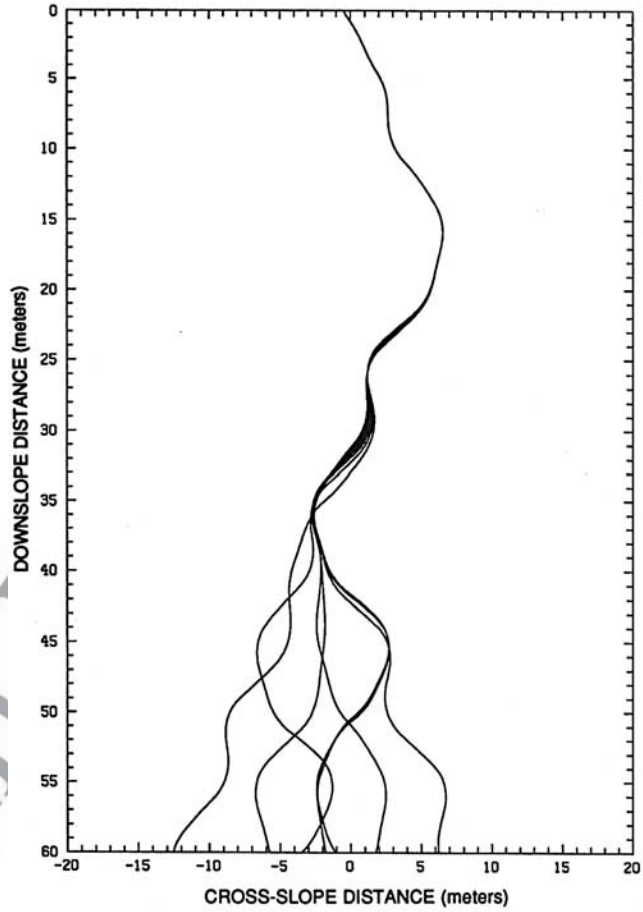

Figure 1. The paths of seven sliding boards down a slope, starting with identical velocities from points spaced at 1-mm intervals, demonstrating an essential property of chaotic behavior: Nearby states will eventually diverge no matter how small the initial difference is [*Lorenz*, 1997].

2.1.4. Feedback and Emergent Systems

[17] If a process X affects a process Y such that Y in turn affects X, the system has feedback. To predict the behavior of such a system, both relationships between X and Y and between Y and X should be studied simultaneously. A typical feature of nonlinear dynamic systems with feedback is the development of some emergent higher-order (macroscopic) structures, which might be caused by lower-level (local or microscopic) dynamics of the system [*Blitz*, 1992; *Baas and Emmeche*, 1997]. If one assumes that a

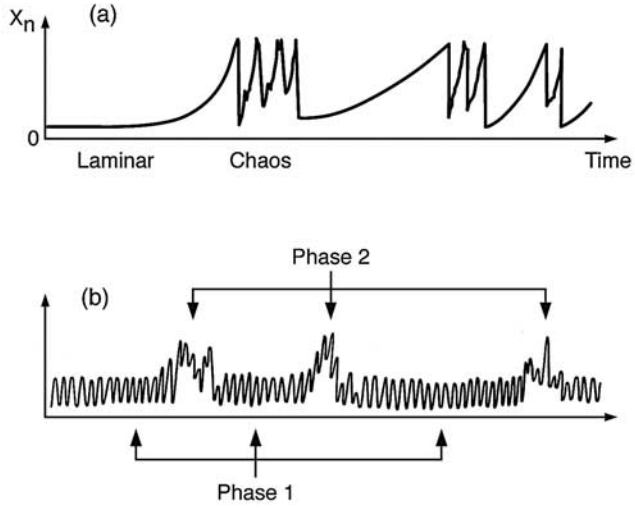

Figure 2. Examples of time series data exhibiting different types of an intermittency route to chaos: (a) a signal alternates between laminar (monotonic) phases and relatively short chaotic bursts [*Schuster*, 1988] and (b) a signal alternates between the long-term quasiperiodic fluctuations (phase 1) and short-term (phase 2) fluctuations (called a collapse of quasiperiodicity [*Rabinovich and Trubetskov*, 1994]).

process depends on interaction of system's components (e.g., particles), then a new process (developed under new boundary conditions) will map each system's component to its new distinct value, so that a new process becomes emergent. Thus the interaction of the system's components (subsystems) creates emerging patterns in the system's behavior. Emergent structures, in turn, control the macroscopic behavior of the system. A notion of emergence can also be considered from the point of view of a hierarchical system, in which the emergent patterns on higher levels are arising from those on lower levels of the system. Simple examples of the emergence are the following: (1) Individual molecules do not have temperature or pressure as a whole system, (b) collective oscillations in ecosystems are different from those of processes in plants or soils, and (3) flow and transport in fractured rock on a regional scale are different from those for liquid flow and chemical interactions in fractures and the matrix (on a lower level). The spontaneous emergence of complex and often surprising macroscopic structures could result from the collective behavior of local-scale processes. In a system with collective behavior, macroscopic, spatially averaged, and time-averaged processes evolve independently, without direct influence on microscopic chaotic dynamics. Chaotic processes, which develop on a small scale and evolve into some kind of collective (volume or time averaged) behavior, can be described using a few variables [*Chaté et al.*, 1996].

2.1.5. Instability

[18] Instability is the condition of a system easily disturbed by internal or external forces or events and which may not return to its previous condition, such as a system with an irreversible hysteresis. Instability is a characteristic of a system far from equilibrium, which is developed under the influence of both internal and external factors.

2.2. Phase Space Reconstruction of Nonlinear Dynamical Systems From Time Series Data

2.2.1. Phase Space and Attractor

[19] One of the most powerful techniques for the time series analysis is the phase space reconstruction. The phase space of a dynamic system is defined as an n-dimensional mathematical space with orthogonal coordinates representing the n variables needed to specify the instantaneous state of the system [*Baker and Gollub*, 1996]. The trajectories of the system's vector in the n-dimensional phase space evolve in time from initial conditions onto the geometrical object called an attractor. The attractor is a set of points in a phase space toward which nearly all trajectories converge, and the attractor describes an ensemble of states of the system. For a dynamic process, which is described by a system of evolution equations, the coordinates of a phase space are state variables or components of the state vector [*Moon*, 1987], so that the evolution of a system is described without direct time-dependent dynamic variables.

[20] Different variables can be used as the coordinates to graphically construct the attractor in the phase space, which provides no explicit relationship of the variable versus time. Examples are (1) the relationship between different system parameters (e.g., directly measured physical variables such as capillary pressure, moisture content, and flow rate) (it is said that the attractor is plotted in the parameter space), (2) the one-dimensional scalar array [*Abarbanel*, 1996], $X_i(t)$, of one of the physical variables (e.g., time series of pressure, temperature, velocity, or saturation array) and its first and second derivatives, and (3) the scalar data, $X_i(t)$, and the values $X_i(t + \tau)$ and $X_i(t + 2\tau)$, separated by a time delay, τ, between successive measurements (this procedure is called a pseudo phase space reconstruction).

[21] The bounds of the attractor characterize the range of system parameters within which the system behaves. Some nonlinear dissipative dynamic systems converge toward attractors on which the trajectories are aperiodic, i.e., chaotic. Such attractors are called strange, or chaotic, attractors. The chaotic attractor has the following properties: (1) Adjacent trajectories in the phase space of the attractor diverge exponentially with time. (2) The attractor trajectories exist in d-dimensions (a minimum of three dimensions in the phase space is required for a chaotic attractor to exist. (3) Trajectories on the attractor are not closed; that is, a single trajectory will never return to an initial point but will visit all points of the attractor in infinite time.

[22] To illustrate the difference between the attractors for deterministic chaotic and random systems, Figure 3 presents three three-dimensional (3-D) attractors in a pseudo phase space, using the relationships between the value of the time-varying function at time t and its values at times $t + \tau$ and $t + 2\tau$. Figures 3a and 3b demonstrate a deterministic chaotic time series and the attractor, respectively, for the

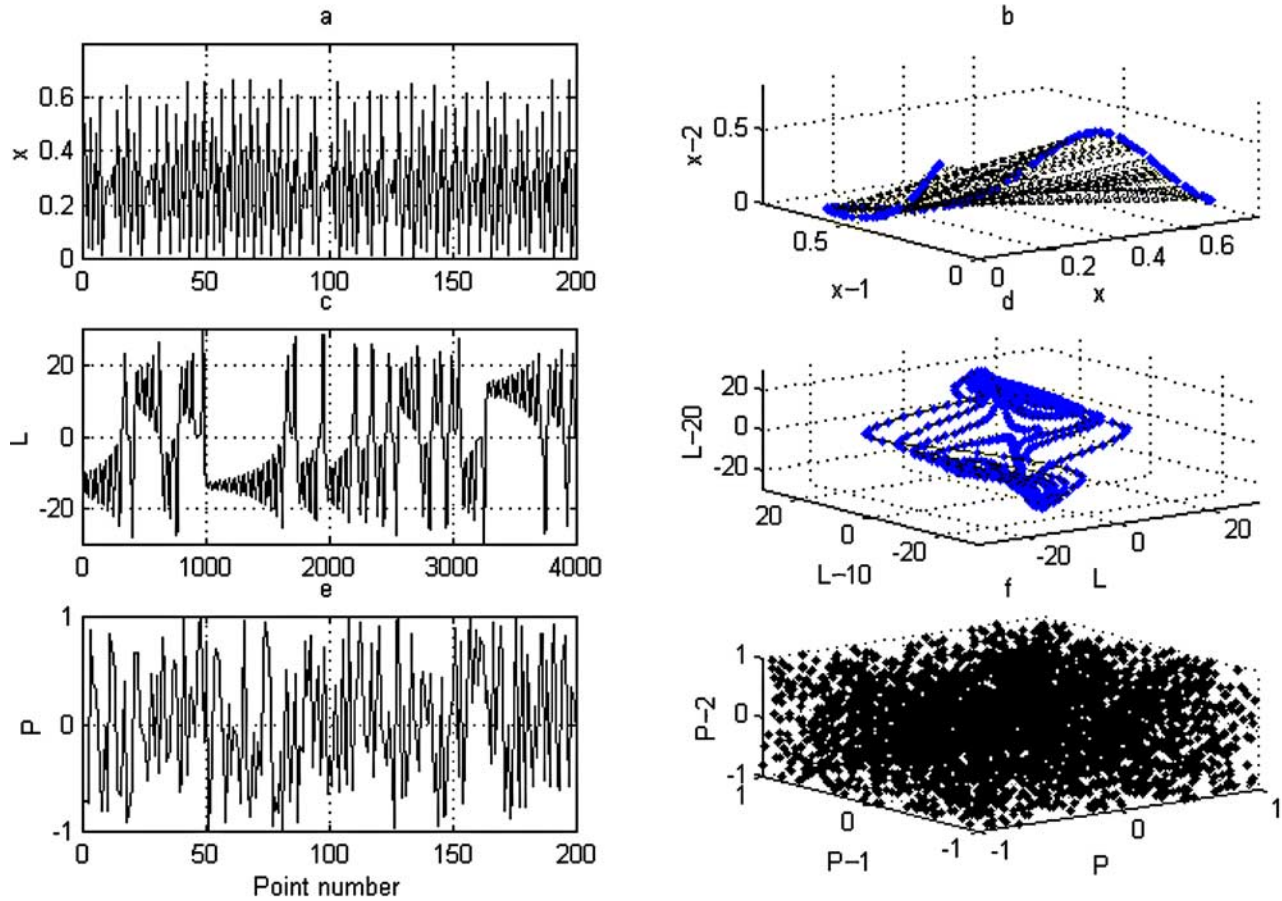

Figure 3. Examples of (left) time series functions and (right) corresponding three-dimensional (3-D) attractors, representing the relationships between the value of the time-varying function at time t and its value at time $t + \tau$. (a) Time series and (b) attractor of the solution of the exponential function (see equation (16), with $A = 20$ and $\alpha = 11$), where $\tau = 1$. (c) Time series and (d) attractor of the solution of deterministic chaotic Lorenz equations with the attractor showing a specific well-defined pattern with two twisted loops, where $\tau = 10$. (e) Time series and (f) attractor of a random function, covering the whole three-dimensional phase space, where $\tau = 1$.

solution of a simple exponential function (see equation (16) in section 2.3.2). Figures 3c and 3d show that a time series of the well-known deterministic chaotic Lorenz model has an attractor with a specific twisted loop pattern. Figures 3e and 3f illustrate that for a random function the attractor covers the whole three-dimensional phase space. It is intuitively apparent from Figure 3f that the unstructured scatter of the points, which make up the attractor, characterizes the contribution of a random component. An analysis of a nonlinear dynamical system, using one-dimensional observations of a scalar signal, includes the determination of several time series and diagnostic parameters of chaos [*Abarbanel*, 1996].

2.2.2. Time Domain Analysis

[23] Fourier transformation is a conventional method of analyzing time series data to determine the power (mean square amplitude) as a function of frequency. Periodic and quasiperiodic data produce a few dominant peaks in the spectrum, while deterministic chaotic and random data produce broad spectra. The autocorrelation function can be used to qualitatively determine the presence of periodicity (cyclic fluctuations), randomness, or deterministic chaotic behavior in the time series data [*Nisbet and Gurney*, 1982] and to determine the delay time [*Sprott and Rowlands*, 1995]. Figure 4a gives an example of the autocorrelation function for the solution (Figure 3a) of the exponential equation exhibiting a phase-forgetting fluctuation. Figure 4b shows that the autocorrelation function for the Lorenz model (plotted in Figure 3c) decreases gradually, which is typical for noncyclic fluctuations [*Nisbet and Gurney*, 1982]. Figure 4c demonstrates that the autocorrelation function for a random time series (plotted in Figure 3e) abruptly drops to zero.

[24] The Hurst exponent, H, is a characteristic of the "fractality," or persistence, in time series. The notion of the Hurst exponent arises within the context of nonstationary stochastic process with stationary increments [*Molz and Liu*, 1997], also called stochastic fractals. H is related to the type of autocorrelation in the time series or spatial series of the stationary process, with $0 \leq H \leq 1$. The value of $H = 0.5$

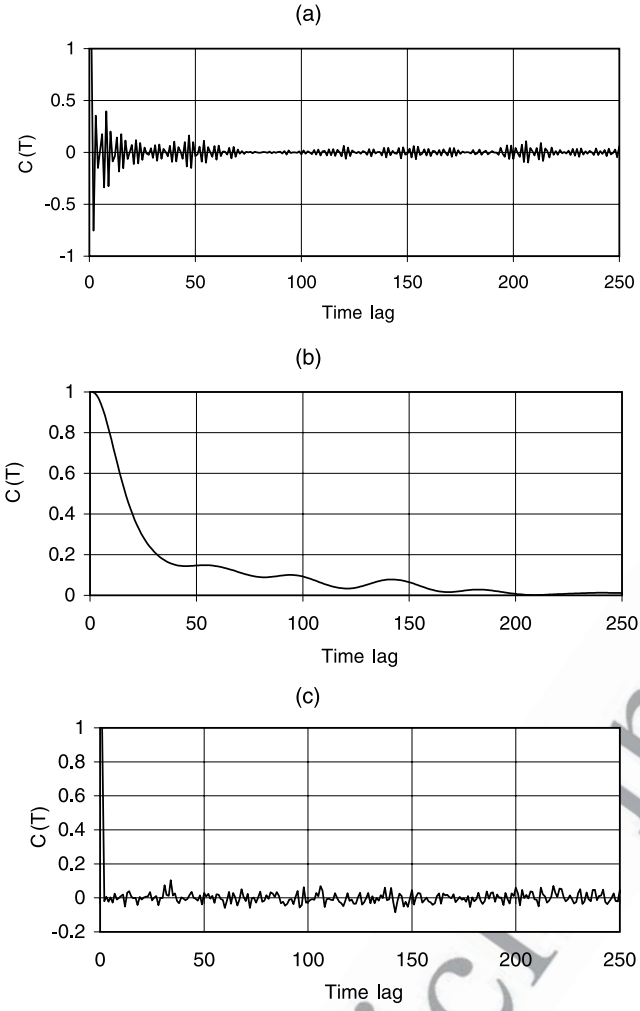

Figure 4. Autocorrelation functions for the (a) time series shown in Figure 3a, illustrating an example of phase-forgetting oscillations; (b) time series of the Lorenz model shown in Figure 3c, illustrating a gradual decrease typical for noncyclic fluctuations; and (c) random time series shown in Figure 3e, illustrating the abrupt drop to zero.

characterizes an uncorrelated process (Brownian motion or Gaussian noise), with successive steps being independent. $H < 0.5$ yields a negatively correlated stochastic process, and $H > 0.5$ characterizes a positively correlated process. As H increases toward 1, the stochastic process becomes less irregular, with better defined trends, implying improved near-term predictability of the system behavior.

[25] As a chaotic system may include both noisy and deterministic chaotic components, it is important to discriminate these components [*Kapitaniak*, 1988; *Williams*, 1997; *Dubois*, 1998]. For this purpose, in general, we can employ either a high-pass filter (which removes low-frequency fluctuation and allows high-frequency fluctuations to pass) or a low-pass filter (which removes high-frequency fluctuation and allows low-frequency fluctuations to pass). In the examples presented in this paper, we employed the Fourier transform method (using a code distributed by *TruSoft International*, *Inc.* [1997]) based on the modification of the transform coefficients with the following reverse transform, thus removing data points contributing uncorrelated noise to the data set.

2.2.3. Diagnostic Parameters of Chaos

[26] Contrary to the Fourier analysis and the autocorrelation function, which directly analyze the time series data of the observed scalar signal (e.g., measured pressure, temperature, and flow rate), the chaotic analysis of nonlinear systems is conducted in the n-dimensional phase space, for example, using time-lagged physical variables characterizing the system. In reconstructing the phase space of a system we determine the following main diagnostic parameters of chaos [*Tsonis*, 1992; *Abarbanel*, 1996]: correlation (delay) time (τ), global embedding dimension (D_{GED}), local embedding dimension (D_L), capacity (fractal) dimension (D_{cap} or D_0), correlation dimension (D_{cor} or D_2), Lyapunov exponents (λ_{Lyap}), and Lyapunov dimension (D_{Lyap} or D_1). In calculating these parameters we used a code CSPW (Contemporary Signal Processing for Windows, csp W, Software, Version 1.2) [*Abarbanel*, 1996], except D_{cor}, which was calculated using the code CDA Pro (Chaos Data Analyzer: The Professional Version) [*Sprott and Rowlands*, 1995].

[27] Correlation (delay) time is the time between the discrete time series points when a correlation between the point values essentially vanishes. The correlation time is determined using the average mutual information function based on *Shannon and Weaver*'s [1949] mutual information [*Gallager*, 1968; *Abarbanel*, 1996]. (Note that using the autocorrelation function may significantly overestimate τ.)

[28] Global embedding dimension, D_{GED}, is the minimum (optimum) embedding dimension for phase space reconstruction. The global embedding dimension is determined using a method called false nearest neighbors (FNN) [*Kennel et al.*, 1992]. Using the FNN method, we determine the fraction of "false neighbors" (the points apparently positioned close to each other because of projection and which are separated in higher embedding dimensions) as a function of the embedding dimension that is needed to unfold an attractor. In other words, for the D_{GED}-dimensional attractor the nearest neighbors along the attractor trajectories do not move apart significantly and cross each other compared to the next higher embedding dimension.

[29] Local embedding dimension, D_L, characterizes how the dynamic system evolves on a local scale [*Abarbanel*, 1996]. D_L indicates the number of degrees of freedom governing the system dynamics, i.e., how many dimensions should be used to predict the system dynamics [*Abarbanel and Tsimring*, 1998], and $D_L \leq D_{\mathrm{GED}}$.

[30] Correlation dimension, D_{cor} (sometimes named D_2), is a scaling exponent characterizing a cloud of points in an n-dimensional phase space given by [*Grassberger and Procaccia*, 1983a, 1983b]

$$C(r) \sim r^{D_{\mathrm{cor}}} \tag{6a}$$

or

$$C(r) = 1/N^2 \; \Sigma H_f\left(r - \left|x_{\mathrm{i}} - x_{\mathrm{j}}\right|\right), \tag{6b}$$

where $C(r)$ is the number of pairs separated by distances less than r, N is the number of points, and H_f is the Heaviside function, which takes the value of 1 if $(r - |x_i - x_j|) > 0$ and 0 otherwise.

[31] Lyapunov exponents are the most valuable diagnostic parameters needed to identify a chaotic system. The Lyapunov exponents are a measure of the divergence with time of initially adjacent trajectories in the phase space. The number of Lyapunov exponents equals the local embedding dimension D_L.

2.2.4. Number of Points for Chaotic Analysis

[32] There is no general rule to determine the needed number of data points for a chaos analysis [*Williams*, 1997]. The minimum number of points to produce an error of no more than $0.05n$ (for 95% confidence) for $n < 20$ (where n is the embedding dimension) in calculating D_{cor} can be determined from [*Tsonis*, 1992]

$$N_{min} \sim 10^{2+0.4n}. \quad (7)$$

From equation (7), for example, for $n = 4$ the minimum number of points is ~4000, and for $n = 5$ it is 10,000 points. Using fewer points, the attractor dimension can be underestimated [*Lorenz*, 1991; *Tsonis*, 1992]. In the presence of noise the attractor dimensions can be overestimated, as the noise itself behaves as an infinite-dimensional system that diffuses the fractal structure of the attractor [*Kapitaniak*, 1988].

2.3. Models of Nonlinear Dynamics and Chaos

2.3.1. Types of Phenomenological Models

2.3.1.1. Hierarchical Scales

[33] A common equation used to describe flow in a fully saturated fracture is a cubic law [*Witherspoon et al.*, 1980]. However, a combination of many nonlinear factors and processes on a local scale in a fracture leads to the departure from the cubic law even in a single fracture [*Pyrak-Nolte et al.*, 1995]. One of the alternative approaches for the problem of modeling is based on the concept of a hierarchy of scales. A conventional hierarchical approach [e.g., *Wheatcraft and Cushman*, 1991; *Neuman and Di Federico*, 1998; *Doughty and Karasaki*, 2002] presents an infinite hierarchy of scales for a permeability field, implying that the same partial differential equation describes flow processes on different scales, with differences arising from the effect of using different properties at different scales. Contrary to this approach, a hierarchical approach by *Faybishenko et al.* [2001b, 2003a] assumes different phenomenological models for different hierarchical scales. These hierarchical scales are as follows: (1) elemental scale, laboratory cores, fracture replicas, or a single fracture at a field site; (2) small scale (approximately 0.1–1 m^2), representing flow and mass transport in a single fracture, including the fracture-matrix interaction, film flow, and dripping water phenomena; (3) intermediate scale (approximately 10–100 m^2), representing flow in the fracture network on a field scale; and (4) large (regional) scale, representing the fracture and fault network geometry.

[34] The need for different models for different levels of the hierarchy arises from the fact that we normally use various instrumentation and methods depending on the scale of observations or measurements. For example, on the elemental scale, using fracture replicas, we can observe intrafracture water meandering and dripping [*Su et al.*, 1999; *Geller et al.*, 2001], depending on the fracture roughness, which are not observable at larger scales. On the small field scale, using small infiltration tests, we can measure the infiltration flux into a single fracture and the surrounding matrix, as well as water dripping frequency from the fracture [*Podgorney et al.*, 2000], which are not usually observable either at larger or smaller scales. On the intermediate scale we can conduct an infiltration test characterizing flow and transport in a fracture network [*Faybishenko et al.*, 2000], which physically may differ from the results of measurements in a single fracture or a fracture core and replica. On the large field scale we study the effects of geologic features, for example, faults or rubble zones, which are neither geometrically nor physically analogous to smaller-scale investigations. Because the model type depends on the scale, to obtain spatially aggregated predictions at a larger scale, the smaller-scale model should be run at multiple locations, allowing the aggregation of model outputs.

2.3.1.2. Elemental-Scale or Small-Scale Models

[35] Using measurements of different state variables (such as pressure, temperature, or concentration) at the same location, a general form equation for the system's state vector for a given time is given by

$$\mathbf{q} = f(q_1, \ldots, q_k), \quad (8)$$

where $q_i (i = 1, \ldots, k)$ represents different state variables. Using the time series of a variable, a discrete scalar time series deterministic model can be presented as

$$x_{n+1} = N(x_n), \quad (9)$$

where subscript n denotes discrete time steps and N is a nonlinear function, which can also be a vector [*Lai and Chen*, 1996; *Haken*, 1997]. In the presence of a random variable (η_n), with the expected value $E(\eta_n) = 0$, the model becomes

$$x_{n+1} = N(x_n) + \eta_n. \quad (10)$$

The application of this model using the results of the water-air injection test is given in section 4.1.

2.3.1.3. Intermediate- or Large-Scale Models

[36] The space- and time-dependent state vector of the system variable (quantity), $\mathbf{q}$, can be presented as

$$\mathbf{q} = f(\mathbf{x}, t), \quad (11)$$

where $f(\mathbf{x}, t)$ could refer to either a scalar variable (e.g., pressure, temperature, and concentration) or flow through the material. The general form of the evolution (balance)

equation for a certain area, depth, and time intervals can be given by

$$q_c = q_p - q_l. \tag{12}$$

where q_c is the rate of change of $\mathbf{q}$, q_p is the production rate of $\mathbf{q}$, and q_l is the loss rate of $\mathbf{q}$. Taking into account both nonlinear deterministic and stochastic components of $\mathbf{q}$, equation (12) can be presented as [*Haken*, 1983, 1997]

$$\mathbf{q}'(\mathbf{x},t) = \mathbf{N}[\mathbf{q}(\mathbf{x},t),\mathbf{x},\nabla,\alpha,t)] + \mathbf{F}(\mathbf{x},t), \tag{13}$$

where $\mathbf{N}$ is a nonlinear function, $\mathbf{q}'$ is the temporal derivative of $\mathbf{q}$, $\mathbf{x}$ is the space variable, $\mathbf{F}(\mathbf{x},t)$ is a fluctuating external force, and α is a control parameter.

2.3.1.4. Time Delay Equation

[37] If the delay time (τ) is known, which is typical for systems with a feedback, a simplified form of equation (13) can be given by a delay equation

$$q'(t) = N[q(t-\tau)]. \tag{14}$$

Delay equations can be used in either time series or evolution models (see section 2.3.2). Note that the initial condition used in solving the delay equation should be fixed for the time interval τ [*Haken*, 1997]. The solution of the delay model from a single data series can be provided using a phase reconstruction method (see section 2.2).

2.3.2. Difference Equation for a Time Series Model

[38] Discrete time series chaotic models (derived as an approximation of simple continuous analytical functions) are extensively used in population dynamics [*May*, 1981]. For example, from the exponential function

$$y = Ax\exp(-\alpha x), \tag{15}$$

where A and α are coefficients, one can obtain the difference equation

$$x_{n+1} = Ax_n\exp(-\alpha x_n). \tag{16}$$

The investigation of equation (16) shows that as A increases, the function $x_{n+1} = f(x_n)$ goes from a stable state to cycling, period doubling, and then to chaos. Equations (15) and (16) were used to describe the time series data in population dynamics [*May*, 1981; *Sparrow*, 1982]. An application of equation (16) with a random component for flow in a fracture will be given in section 4.1.

2.3.3. Difference-Differential Equation for Soil Moisture Balance

[39] On the basis of the general form of the balance equation, equation (12), the equation for long-term soil moisture variations within a certain area and representing a hydrologically active depth interval, can be written as [*Rodriguez-Iturbe et al.*, 1991a, equation (1)]

$$nZ_r\, ds/dt = P(s)\phi(s) - E(s), \tag{17}$$

where n is the soil porosity, Z_r is the hydrologically active depth interval, s is the moisture saturation, t is time, $P(s)$ is the precipitation rate, $\phi(s)$ is the infiltration function (characterizing the fraction of precipitation causing infiltration), and $E(s)$ is the evapotranspiration rate. Equation (17) expresses the feedback between atmospheric and subsurface flow processes. *Rodriguez-Iturbe et al.* [1991a, 1991b] assumed the following relationships between infiltration, precipitation, and evapotranspiration rates as functions of soil saturation:

$$E(s) = E_p s^c, \tag{18}$$

$$\phi(s) = 1 - \varepsilon s^r, \tag{19}$$

$$P(s) = P_a(1 + s^c/A_c), \tag{20}$$

where E_p is the potential evapotranspiration and c, ε, and r are nonnegative constants, P_a is an advective component of precipitation resulting from the external (advective) water vapor formed by evaporation outside the given area, for which equation (17) is written, and A_c is a parameter describing the combined effect of the advective moisture influx to the study area, wind speed, and potential evaporation. To take into account the dynamic effect of the moisture content on infiltration, *Rodriguez-Iturbe et al.* [1991b] introduced a delay mechanism into the equation for soil moisture dynamics representing timescales from a week to 2–3 months. As a result, they developed a difference-differential equation:

$$ds(t)/dt = \alpha s(t-\tau)/[\beta + s^m(t-\tau)]\ \ \{a[1 + s^c(t-\tau)/A]\}\phi[s(t)] - bs^c(t), \tag{21}$$

where $s(t)$ is the soil saturation at time t, τ is the time delay interval, $s(t-\tau)$ is the saturation at time $(t-\tau)$, m, α, and β are positive coefficients, and $a = P_a/(nZ_r)$ and $b = E_p/(nZ_r)$ are independent climatic forcing coefficients [*Rodriguez-Iturbe et al.*, 1991a]. Thus, instead of a one-dimensional differential equation, equation (17), a delayed difference-differential equation, equation (21), representing an infinite-dimensional system, was obtained. Depending on the values of parameters, equation (21) may either converge to a fixed equilibrium point, developing a limit cycle, or converge to any nonperiodic pattern, creating chaotic behavior. Examples of the time series and corresponding attractors generated using the solution of equation (21) are shown in Figure 5.

2.3.4. Partial Differential Equation for Film Flow

[40] Film flow in fractures is controlled by a combination of surface tension, gravity, and inertia. In unsaturated fractures, liquid film is bounded on one side of the fracture by the supporting solid matrix and on the other side by a fluid interface. If the surrounding fluid is gas, the film has a free surface. Film flow processes also depend on numerous factors, such as traces of impurities, roughness, temperature, the contact angle of a drop [*Deriagin et al.*, 1985], and intrafracture water dripping [*Geller et al.*, 2001]. Recent theoretical and computational research [*Swinney*

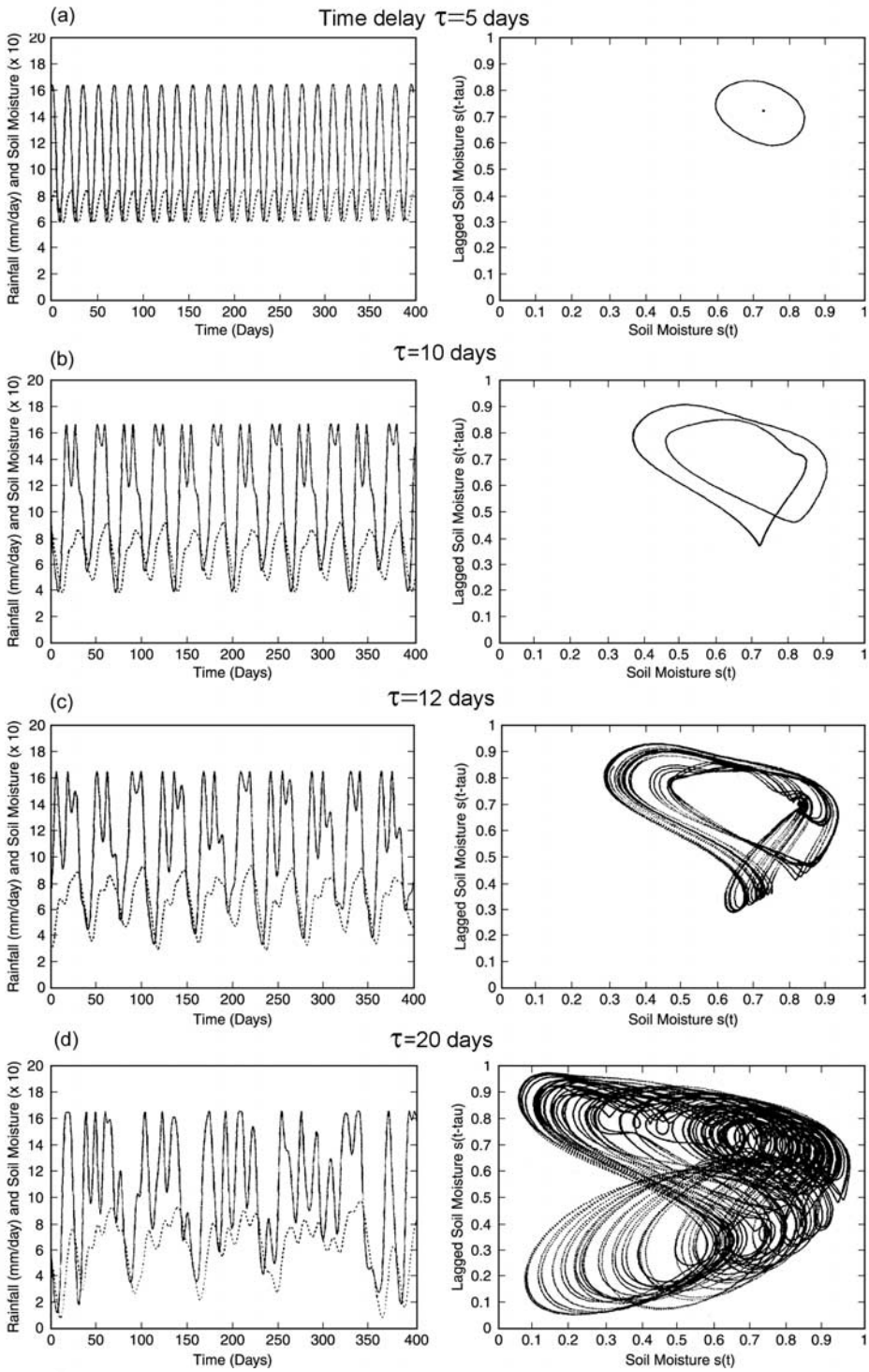

Figure 5. Examples of the solution of equation (21) with different time delays: (a) 5 days, (b) 10 days, (c) 12 days, and (d) 20 days. (left) The time series of the moisture content (dashed lines) and precipitation (solid lines) and (right) corresponding attractors are shown. Adapted from *Rodriguez-Iturbe et al.* [1991b].

and Gollub, 1985; *Indereshkumar and Frenkel*, 1999] on films flowing down inclined planes indicated highly ordered patterns that can spontaneously appear in some driven dissipative systems. For high Reynolds numbers [*Yu et al.*, 1995] the instability is created by gravity forces [*Frenkel et al.*, 1987; *Nicholl et al.*, 1994; *Frenkel and Indireshkumar*, 1996]. For small Reynolds numbers the instability is created by molecular forces [*Faybishenko et al.*, 2001b]. For both large and small Reynolds numbers, film flow on an inclined surface can be described using a fourth-order partial differ-

ential equation, called the Kuramoto-Sivashinsky (K-S) equation, given in a canonical form by [*Frenkel and Indireshkumar*, 1996; *Faybishenko et al.*, 2001b]

$$\frac{\partial \phi}{\partial \tau} + \phi \frac{\partial \phi}{\partial \chi} + \frac{\partial^2 \phi}{\partial \chi^2} + \frac{\partial^4 \phi}{\partial \chi^4} = 0, \qquad (22)$$

where ϕ, χ, and τ are dimensionless film thickness, length, and time, respectively. The gravitational, capillary, and molecular forces included in the derivation of the K-S equation are identical to those occurring in fractures. *Sivashinsky and Michelson* [1980] were the first to indicate that the deterministic equation, equation (22), leads to chaotic behavior. In the K-S equation the second term is a nonlinear term; the third and fourth are the destabilizing and stabilizing terms, respectively, on the same order of magnitude, that describe dissipative processes [*Babchin et al.*, 1983; *Frenkel et al.*, 1987]. Because the attractors of the solution of equation (22) are geometrically analogous to those plotted from the results of laboratory and field experiments (see section 4), we hypothesize that equation (22) could be used to describe intrafracture flow. For the flow process described by the K-S equation, we can reasonably hypothesize that the linear relationship between the pressure head and the flow rate (i.e., Darcy's law) on a local scale is invalid at least for the periods of chaotic fluctuation.

3. KEY FEATURES OF GEOMETRY AND NONLINEAR DYNAMICS OF FLOW THROUGH UNSATURATED FRACTURED POROUS MEDIA

[41] Processes generating nonlinear dynamics in flow through unsaturated fractured porous media can be divided into two categories: (1) the complex geometry of flow paths and (2) nonlinear liquid flow and chemical transport through fractures and surrounding matrix. A key question is, What is the role of internal factors associated with the geometry and physics of unsaturated intrafracture flow (i.e., film flow and water dripping) in causing the chaotic dynamics?

3.1. Complex Geometry of Flow Paths and Conceptual Models of Fracture Networks

3.1.1. Rock Discontinuities

[42] Rock discontinuities are present on all scales, extending from the microscale of microfissures, among the mineral components of the rock, to the macroscale of various types of joints and faults [*da Cunha*, 1993; *Priest*, 1993]. The geometrical structure and physics of flow through fractured rock can be viewed differently depending on the scale of the investigation, which is one of the main reasons for using the concept of scale hierarchy for fractured rock [*Faybishenko et al.*, 2003a].

[43] To provide an example of complexity of geometrical features of fractured rock on a field scale (mesoscale), Figure 6a illustrates a photograph of a fractured-basalt outcrop at the Box Canyon site in Idaho near the Idaho National Engineering and Environmental Laboratory (INEEL). Figure 6 shows a variety of irregular (on average, hexagonal [*Korvin*, 1992]) basalt columns separated by vertical joints and horizontal fractures. The complexity of the fracture network geometry (featuring a decreasing number of conducting fractures with depth) can cause either divergence or convergence of localized and nonuniform flow paths in different parts of the basalt flow and the intersection of flow paths with mixing of the flowing solution (Figure 6b).

[44] The intrafracture flow processes are affected by a variety of local flow patterns for different fracture junctions. For example, *Stothoff and Or* [2000] presented examples of lateral diversion on hanging walls (which is flux-dependent), routing into fractures (which is fracture-capacity-dependent), anisotropy from diversion, and funneling or split flow that may occur as a result of fracture offsets. Moreover, the intrafracture flow processes are affected by the fracture aperture, fracture surface roughness, asperity contacts, and the fracture-matrix interaction [*Pruess*, 1999; *Gentier et al.*, 2000; *Ho*, 2001]. Furthermore, it is apparent that intrafracture roughness affecting flow on a local scale is neither geometrically nor physically analogous to the field-scale fracture pattern.

3.1.2. Intrafracture Flow Fingering and Tortuosity Effects

[45] Laboratory experiments with fracture models [*Glass et al.*, 1989, 1991; *Su et al.*, 1999; *Geller et al.*, 2001] demonstrated the pervasiveness of highly localized and extremely nonuniform flow paths in the fracture plane. In their laboratory tests, using dyed water supplied through a ceramic plate at the top of a transparent fracture replica (about 15 cm wide and 30 cm long) with a variable aperture, *Su et al.* [1999] showed that the local geometry of flow could change rapidly over time. *Geller et al.* [2001] observed similar behavior in dripping-water experiments conducted using a transparent replica of a natural rock fracture with a variable aperture. Fingers are also formed in water-repellent sandy soils [*Ritsema et al.*, 1998]. Once developed, fingers usually progress along the same pathways, and the average coverage of these pathways remains virtually stable over time, confirming the concept of a "self-organized" critical state [*Janosi and Horvath*, 1989].

[46] This concept implies that the nonuniform surface coverage has a critical value even after additional water is supplied to the surface. The system organizes itself in such a way that the additional water is removed through streams, which is confirmed experimentally and by using computer simulations of raindrops on a window pane [*Janosi and Horvath*, 1989]. *Su et al.* [1999] and *Geller et al.* [2001] observed practically the same average coverage of seeps over time, while the local geometry of flow changed rapidly. The results of laboratory studies by *Geller et al.* [2001] are analyzed in section 4.

[47] Intrafracture flow patterns are strongly dependent on tortuosity effects that take place in the fracture space [e.g., *Tsang*, 1984]. Tortuosity effects in intrafracture flow processes are significantly dependent on the asperity pattern,

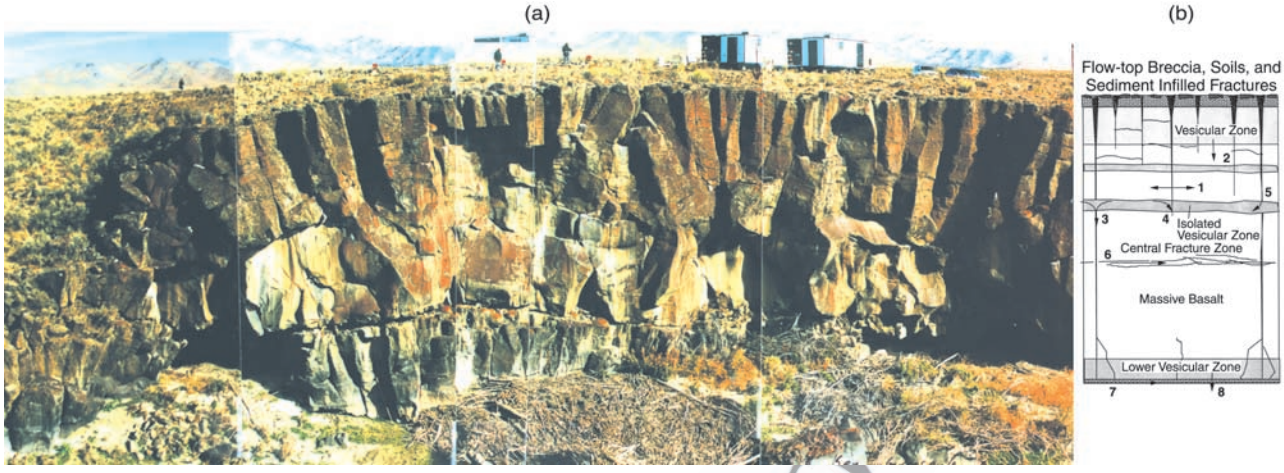

Figure 6. (a) A photograph of a fractured basalt outcrop at the Box Canyon site in Idaho near the Idaho National Engineering and Environmental Laboratory, showing a variety of irregular basalt columns separated by vertical joints and horizontal fractures. (b) Schematic of mechanisms of water flow in fractured basalt: (1) fracture-to-matrix diffusion, (2) vesicular basalt–to–massive basalt diffusion, (3) preferential flow through conductive fractures and the effect of funneling, (4) vesicular basalt–to–nonconductive fracture diffusion, (5) conductive fracture–to–vesicular basalt flow and diffusion, (6) lateral flow and advective transport in the central fracture zone, (7) lateral flow and advective transport in the rubble zone, and (8) flow into the underlying basalt flow [*Faybishenko et al.*, 2000].

which may lead to complex dendritic patterns for the saturation distribution within a fracture during wetting-drying cycles [*Liou*, 1999; *Pruess*, 1999, 2000; *Ho*, 2001].

3.1.3. Temporal Changes in Flow Geometry

[48] Field and laboratory studies revealed that fractures might become nonconductive because apertures could gradually be closed, either partially or completely. For example, in a series of laboratory experiments, *Gentier et al.* [2000] found that as the normal stress increases, the initial value of intrinsic transmissivity is reduced by 1.5–10 times, with the smallest reductions for fractures with hard infill. In field infiltration tests, *Dahan et al.* [2001] found that fracture coating, salt dissolution, particle shearing from the relatively soft fracture surfaces, disintegration of fracture filling materials, solid particle migration, and clay swelling are the main processes causing instability and temporal variation of the flow rate. These intrafracture changes are likely to affect the directions of flow paths as well.

3.1.4. Fracture Network Conceptual Models

[49] Fracture network conceptual models are based on evaluation of fracture length, density, and connectivity. Several studies indicate a power law distribution of either faults [*Bour and Davy*, 1997] or fracture lengths [*Walmann et al.*, 1996; *Renshaw*, 2000]. However, the power law distribution may fail for small scales (less than 10^{-5}–10^{-3} m) or large scales (exceeding 10^{1}–10^{2} m), and the power law exponent may not be constant [*Renshaw*, 2000]. Because water flow in a fracture network embedded in a low-permeability matrix depends strongly on the interconnections of fractures, fracture-network connectivity is one of the main factors affecting mass transport through rock [*La Pointe*, 2000]. Whereas exact measurements of fracture lengths or connectedness are impossible, field measurements of permeability can be used to determine effective two- or three-dimensional fracture network connectedness [*Renshaw*, 2000]. A shortcoming of network models is that the fracture geometric parameters strongly impacting flow and transport, such as fracture apertures and connectivity, typically cannot be well constrained from field observations [*Pruess et al.*, 1999].

[50] Fractal analysis has been used to predict the fractal structure and flow parameters in soils and rocks, including the geometry and pore size distribution in the porous space of soil and fractured media, predicting permeability and soil water retention and transport processes such as diffusion, dispersion, adsorption on irregular surfaces, and propagation of cracks and fragmentation [*Barton and Larsen*, 1985; *Carr*, 1989; *Pyrak-Nolte et al.*, 1992; *Tyler and Wheatcraft*, 1990; *Meakin*, 1991; *Sahimi*, 1993; *Crawford et al.*, 1999; *Long et al.*, 1993; *Feder and Jøssang*, 1995; *Molz and Boman*, 1995; *Perrier et al.*, 1996; *Perfect*, 1997; *Pachepsky and Timlin*, 1998]. Fractal and scaling models may also be used to describe the moisture content distribution in heterogeneous media [*Lenormand and Zarcone*, 1989; *Pruess*, 1999, 2000; *Yortsos*, 2000]. In his review of fractal models, *Perfect* [1997] considered the fragmentation of aggregates composed of heterogeneous brittle earth materials of finite size. He assumed that a structural failure is hierarchical in nature and involves multiple fracturing of the aggregate blocks. Despite the fact that many authors have conducted experimental investigations of fractal properties of porous media [e.g., *Rieu and Sposito*, 1991; *Giménez et al.*, 1997], *Perfect* [1997, p. 196] suggested that "while fractal models for the fragmentation of rocks and soils are relatively well developed, their experimental verification is weak or entirely lacking." Also, it is still unclear how well fractal models predict permeability and transport in the subsurface [*Giménez et al.*, 1997; *Doughty and*

Karasaki, 2002]. It is important that the presence of a fractal structure of a fracture network is indicative of an expected chaotic behavior for flow in the subsurface [*Dubois*, 1998; *Turcotte*, 1997].

[51] Models for fracture pattern have limitations in investigating unsaturated flow, because observable fractures often play no significant role in water flow, even when they appear to be geometrically interconnected [*Faybishenko et al.*, 2000; *Glass et al.*, 2002]. To account for fractures affecting flow, *Liu et al.* [1998] proposed an active fracture model for unsaturated flow and transport in fractured rock, assuming gravity-dominated, nonequilibrium, preferential liquid flow in fractures, and a reduced area of fracture-matrix interaction. They inferred that active fractures constitute about 18–27% of the connected fractures in highly fractured tuff under ambient conditions. Moreover, flow paths in partially saturated rocks are not exactly repeatable, because they depend on small variations in boundary and initial conditions [*Faybishenko et al.*, 2000; *Faybishenko*, 2002].

3.2. Processes Causing Nonlinear Dynamics and Flow Instabilities

[52] Nonlinear dynamics in flow through fractured rock results from a nonlinear superposition, competition, and feedback between various factors and processes (most of which are nonlinear), such as fast, preferential flow, episodic flow events, film flow along fracture surfaces, intrafracture dripping water phenomena, fracture-matrix interaction, root uptake, colloidal transport, microbiological activities, temperature effects and vapor transport, entrapped air, chemical transport, chaotic mixing, and sensitivity to initial conditions and flow parameters.

3.2.1. Fast, Preferential Flow and Episodic Flow Events

[53] Fast, preferential flow is one of the most important features of flow in fractured rock. Several attempts have been made to explain the phenomena of fast water seepage in fractured rock using concepts of film flow [*Tokunaga and Wan*, 1997], water channeling [*Johns and Roberts*, 1991; *Pruess*, 1999; *Pruess et al.*, 1999; *Su et al.*, 1999], and fingering [*Selker et al.*, 1992]. Water channeling in fractures limits diffusive coupling between the fracture and matrix to a small area of the fracture plane [*Dykhuizen*, 1992; *Su et al.*, 1999].

[54] Episodic flow events are observed at all scales but particularly at a laboratory scale and are caused by a combination of physical processes resulting, for example, from pore throat and preferential flow effects, surface wettability, fracture roughness, and asperity contacts. Numerous examples of flow instability and episodic flow in both soils and fractured rock are described in the literature. For example, the flow rate [*Prazak et al.*, 1992; *Podgorney et al.*, 2000; *Salve et al.*, 2002] and capillary pressure [*Selker et al.*, 1992] exhibit significant high-frequency temporal fluctuations under constant boundary conditions during infiltration into the subsurface. Air compression ahead of the wetting front creates a pulsation of water pressure at the wetting front [*Wang et al.*, 1998]. Heterogeneous fracture asperities are possible causes for episodic flow events, even under steady-infiltration boundary conditions [*Ho*, 2001]. That asperities create "pinch point" apertures is shown to (in turn) create an intrafracture capillary barrier effect, thus generating episodic accumulation and relatively short drainage events, which are, however, large in magnitude relative to infiltration events within the fracture [*Ho*, 2001].

3.2.2. Film Flow

[55] For partially saturated flow in a fracture the liquid water layer is bounded on one side by the supporting solid matrix and on the other side by air (a free surface). Liquid film flow in fractures is affected by a combination of surface tension, gravity, and inertia. It also depends on numerous other factors, such as traces of impurities, roughness, temperature, and the contact angle of drop [*Deriagin et al.*, 1989], intrafracture water dripping [*Geller et al.*, 2001], grain-grain contacts, salinity, and mineralogy [*Renard and Ortoleva*, 1997]. *Tokunaga and Wan* [1997] determined that the average surface film thickness in fractured tuff ranged from 2 to 70 μm, whereas an average film velocity ranged from 2 to 40 m/d, $\sim 10^3$ times faster than that of the pore water under unit gradient saturated flow.

3.2.3. Dripping Water

[56] It is known that dripping from a single faucet [*Shaw*, 1984] or capillary under controlled boundary conditions is a deterministic chaotic process. Dripping water frequency can be described by a simple logistic difference equation with a small noise component [*Shaw*, 1984] or a one-dimensional approximation of the Navier-Stokes equations [*Ambravaneswaran et al.*, 2000]. We can easily imagine dripping from a fracture as a multifaucet dripping process, which is expected to generate a more complex chaotic process at the fracture exit, compared to a single faucet. However, it is not known whether intrafracture flow processes are chaotic. Intrafracture water dripping is affected by the viscosity, surface tension, and phase changes along an irregular surface, along with sticking, spreading, tortuosity, accumulation and episodic flow of water droplets, impurities, roughness, temperature, and the surface slope. All these processes cause a transition to high-dimensional chaos ($D_{cor} > 5$ [*Sprott and Rowlands*, 1995]), which is difficult to distinguish from randomness. Some examples from laboratory and field dripping-water experiments are given in section 4.

3.2.4. Fracture-Matrix Interaction

[57] Fracture-matrix interaction involves the water exchange between fractures and the surrounding matrix. Fast flow in high-permeability fractures can be retarded by matrix imbibition, causing the variability of flow geometry and moisture content between the matrix on either side of the fracture [*Faybishenko and Finsterle*, 2000]. Because of flow channeling through variably saturated fractures an effective fracture surface area, affecting the fracture-matrix water interaction, is usually less than the total fracture surface [*Geller et al.*, 2001; *Glass et al.*, 1989, 1991; *Glass and Nicholl*, 1996]. Using the results of several case studies

(testing metal plates with irregular geometry surfaces) and laboratory water-dripping experiments (conducted by *Geller et al.* [2001]), *Fuentes and Faybishenko* [2004] have recently shown that the fracture flow area can be predicted from the fracture surface geometry. Fracture-matrix interaction is further complicated by the nonequilibrium nature of the imbibition process, exemplified by spontaneous countercurrent capillary imbibition [*Barenblatt et al.*, 2002]. However, direct field measurements of the fracture-matrix interaction area are impossible to obtain. This area can be estimated using numerical simulations of the results of infiltration tests. For example, according to the three-dimensional modeling of the Box Canyon pneumatic and infiltration tests, using a dual-permeability model, the fracture-matrix interfacial area should be scaled by a factor of 0.01 for the results of modeling to match experiments [*Unger et al.*, 2004].

3.2.5. Root Uptake

[58] *Lai and Katul* [2000] showed that a root water uptake affects the dynamics of soil evapotranspiration, and it depends on preferential water flow through the topsoil layers and extraction from deeper layers despite limited rooting density with depth. To model the water balance in the near-surface zone, we need to account for the dynamic switching of root uptake as a function of soil moisture content and its spatial distribution in the soil profile, which, in turn, may result in chaotic behavior for flow in the root zone.

3.2.6. Microbiological Activity

[59] Feedback between microbiological activity and water flow is an important process, one that affects other vadose zone processes. First, microbiological activity is accelerated as water saturation increases [*Gerba and Goyal*, 1985]. As microorganisms consume relatively insoluble O_2 from soil air [*Garner et al.*, 1969], they produce highly soluble CO_2 [*Flühler et al.*, 1986]. The dissolution of CO_2 decreases the volume of entrapped gas, causing hydraulic conductivity to increase up its the maximum value. In contrast, as microbial cells grow, "biofilms" progressively accumulate, decreasing pore diameters and/or pore throats [*Cunningham*, 1993] and making the particle surfaces irregular (thus increasing the friction factor [*Rittman*, 1993]). As a result, hydraulic conductivity decreases by as much as 3 orders of magnitude [*Cunningham*, 1993; *Jaffe and Taylor*, 1993; *Rittman*, 1993]. The effect of bacterial clogging is much more pronounced in fine-textured materials [*Vandevivere et al.*, 1995]. The sorption and desorption of microbial cells appears to equilibrate with time, resulting in an essentially constant permeability. Entry of free air, containing oxygen, into the soil lessens the effect of biofilms [*Freeze and Cherry*, 1979].

3.2.7. Colloids

[60] The colloidal dynamics in fractured porous media are complicated by the electrokinetic and hydrodynamic interaction between colloids, nonequilibrium adsorption, nonsorptive interactions of bacteria and colloids with particles, growth and grazing by protozoa, and detachment from solid surfaces, which are different from the dynamics in an open space [*Harvey and Garabedian*, 1991]. These processes can be described by a set of nonlinear, coupled electrokinetic and convective diffusion equations for ion densities in combination with Navier-Stokes equations for the mass current [*Horbach and Frenkel*, 2001], indicating that colloidal dynamics are nonlinear [*Pagonabarraga et al.*, 1999].

3.2.8. Temperature and Vapor Transport

[61] Seasonal and diurnal variations in ambient temperature result in subsurface temperature gradients, inducing thermal vapor diffusion [*Milly*, 1996]. Subsurface vapor diffusion affects evapotranspiration, which is controlled simultaneously by root conditions, soil properties, liquid transport, and climatic conditions [*Lakshmi and Wood*, 1998]. The simultaneous vapor and liquid transport in soils presents a kind of feedback mechanism between various controlling parameters, which also affects the interaction of soil moisture and atmospheric processes (Figure 7). *Cahill and Parlange* [1998] showed that in the near-surface zone the contribution of heat flux to vapor transport is significant, accounting for 40–60% of the total moisture flux. To simulate vapor-liquid flow in soil, *Cahill and Parlange* [1998] used Fourier's law for heat flux density and expressed heat transport as a function of mass transfer, accounting for water evaporation in one place and its recondensation in another. They observed a temporal variation of the moisture content with both low- and high-frequency components (Figure 8) and noted that the removal of high-frequency fluctuations could cause some errors in simulations of the water regime. Thermal injection tests in fractured rock are expected to generate more pronounced high-frequency fluctuations of temperature at fractures, whereas the temperature within the rock matrix could change gradually [*Pruess et al.*, 1999].

3.2.9. Chemical Transport

[62] *Turing* [1952] was the first to show that spontaneous patterns observed in biological systems are analogous to those spontaneously occurring in chemical reaction-diffusion systems. The positive feedback between fluid transport and mineral dissolution creates complex reaction front morphologies such as fingers [*Renard et al.*, 1998]. The deterministic chaotic diffusion-reaction process (for assessing the reaction rate in chemical systems) replaces the old stochastic transport models [*Schuster*, 1988; *Gaspard and Klages*, 1998]. According to the deterministic chaotic concept, macroscopic transport coefficients, such as diffusion coefficient and reaction rate, will exhibit irregular behavior as a function of a control system parameter [*Gaspard and Klages*, 1998]. The nonequilibrium and nonlinear processes, typical for self-organizing and nonlinear phenomena, are known to exist at the reaction front [*Ortoleva*, 1994, chapter 6]. These processes result in oscillations, chaos, and waves that have been found to appear at different scales: centimeter-scale redox front scalloping in siltstones, meter- to kilometer-scale scalloping of uranium deposits, submeter-scale weathering fronts in manganese-rich sedimentary rock, dissolution holes in karstified limestones, etc. [*Ortoleva*, 1994, chapter 6]. Figure 9a illustrates the

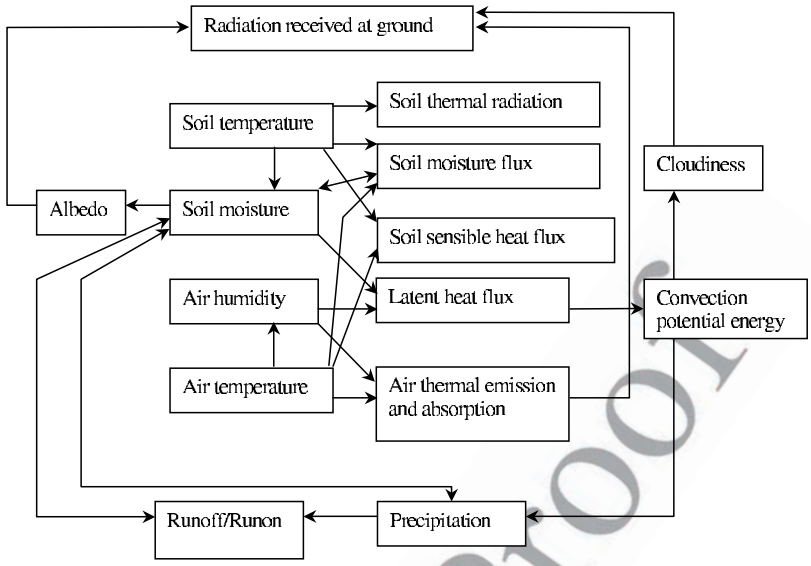

Figure 7. Conceptual diagram of the pathways for the interaction between the soil moisture and precipitation [after *Entekhabi et al.*, 1996].

two-mineral reaction front between the altered and unaltered zones, with the accumulation of mineral B (shaded zones) at tips of dissolution fingers for mineral A, resulting in the oscillatory switching between two configurations. Figure 9b illustrates the possibility of branching of propagating fingers at the reaction front.

3.2.10. Entrapped Air

[63] In groundwater or perched-water zones, entrapped air can be present within the zone of seasonal water table fluctuations. Field and laboratory experimental investigations showed that in the presence of entrapped air, quasi-saturated hydraulic conductivity exhibits a three-stage temporal behavior [*Luthin*, 1957; *Faybishenko*, 1995, 1999], as caused by a nonlinear superposition and competition (i.e., some processes cause the decrease and others cause the increase in hydraulic conductivity) of several processes. During the first stage the hydraulic conductivity decreases as entrapped air redistributes within a porous space and plugs the most conducting pores [*Luthin*, 1957]. During the second stage, as the entrapped air is discharged, hydraulic conductivity increases up to a maximum value at a nearly fully saturated state. Exponential and power law relationships were found to describe the hydraulic conductivity as a function of the volume of entrapped air [*Faybishenko*, 1995]. During the third stage, as biofilms are generated, the hydraulic conductivity eventually decreases to minimum values. When the water table drops, atmospheric air enters the soil, and biofilms are destroyed by oxygen that enters the pore space. During the next infiltration events the initial hydraulic conductivity is high again, which was observed in both soils [*Faybishenko*, 1995] and fractured rocks [*Salve and Oldenburg*, 2001; *Faybishenko et al.*, 2003b]. These temporal fluctuations of the quasi-hydraulic conductivity, K, can be described using a two-threshold logistic differential equation

$$dK/dt = -r(1 - K/K_0)(1 - K/K_s)K \qquad (23)$$

for $K_0 < K_s$, where K_s is the saturated hydraulic conductivity (maximum value of K at the end of the second stage), K_0 is the minimum value of K at the end of the first stage, and r is a parameter that varies for the different stages of percolation.

3.2.11. Chaotic Mixing

[64] Chaotic mixing is the physical process of solute spreading into a fluid, caused by the stretching and folding of material lines and surfaces in heterogeneous media [*Weeks and Sposito*, 1998]. In contrast to dilution, mixing takes place within much shorter timescales, increasing the plume boundary area and causing higher local concentration gradients, thus promoting effective solute dilution. The mixing efficiency generally depends on the spatial variability of hydraulic conductivity (or transitions) between zones of highly contrasting hydraulic conductivities. *Weeks and Sposito* [1998] showed that mixing is driven by unsteady

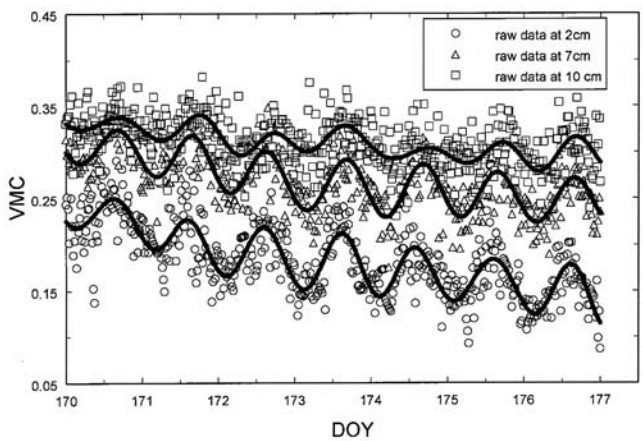

Figure 8. The time series of the volumetric moisture content (VMC) from field observations containing both the low-frequency diurnal fluctuations (solid line) and high-frequency variations (symbols) [*Cahill and Parlange*, 1998].

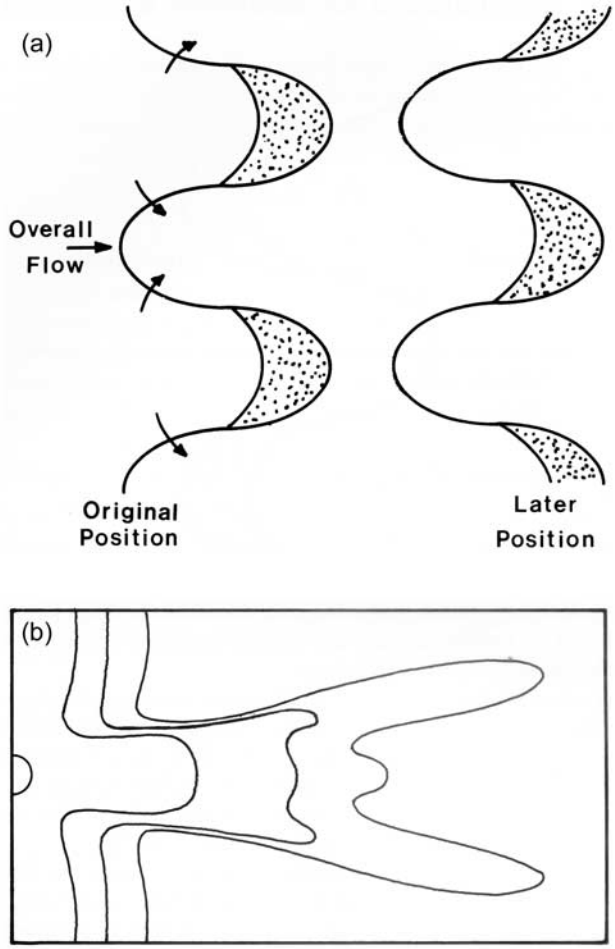

Figure 9. (a) Illustration of the two-mineral reaction front between the chemically altered and unaltered zones with the accumulation of mineral B (shaded zones) at tips of dissolution fingers for mineral A, showing an oscillatory switching between two configurations, and (b) illustration of branching of propagating fingers [*Ortoleva*, 1994, Figures 7–5 and 7–17].

advection, which acts to stretch and fold fluid filaments in such a manner that plume boundary areas become highly irregular. *Weeks and Sposito* [1998] showed that the mixing of a solute plume by unsteady groundwater flow, in an aquifer with pronounced hydraulic conductivity variation, would be most effective if chaotic path lines were induced.

3.2.12. Sensitivity to Initial Conditions and Flow Parameters

[65] Chaotic flow processes in the vadose zone may result from a sensitive dependence of flow parameters upon the coupled effects of several nonlinear intrinsic factors and processes, such as nonlinear relationships between the flow rate, water content, pressure, and temperature; air entrapment; heterogeneity and roughness of fractures; clogging of the conductive fractures by sediments and biofilms; kinetics of the matrix-fracture water exchange; and contact angle hysteresis. As a result, small changes in initial conditions (spatial distribution of water content, pressure, and temperature and pressure, and groundwater fluctuations) may significantly change flow characteristics through unsaturated media. Examples of the sensitivity of flow pathways and the infiltration rate in fractured basalt is given by *Faybishenko et al.* [2000] and *Podgorney et al.* [2000]. Examples of the dependence of hydraulic conductivity on initial moisture content are given by *Hallaire* [1961], *Feldman* [1988], *Conca and Wright* [1994], and *Faybishenko* [1999].

4. EXAMPLES FROM LABORATORY AND FIELD EXPERIMENTS

4.1. Laboratory Experiments to Characterize Intrafracture Flow

4.1.1. Water-Gas Injection Experiments

4.1.1.1. Design of Experiments

[66] *Persoff and Pruess* [1995] conducted a series of two-phase flow experiments by simultaneously injecting water and nitrogen gas, representing wetting and nonwetting phases, respectively, into replicas of natural rough-walled rock fractures of granite (from the Stripa mine in Sweden) and tuff (from the Dixie Valley site, Nevada). In these experiments for each of the constant gas and liquid flow rates the gas and liquid pressure were measured at inlet and outlet edges of the fracture. The analysis of the results of two experiments, experiments A and C, is presented in this section. Experiment A was carried out using a Stripa granite replica (average fracture hydrodynamic aperture 8.5 μm) under a controlled gas/liquid volumetric flow ratio of 9.5, whereas experiment C was carried out using the Stripa natural rock (average fracture hydrodynamic aperture 21.7 μm) with gas flow rate of 0.52 cm^3/min (measured at standard conditions) and liquid flow rate of 15.0 mL/h (the gas/liquid mass flow ratio is 0.025). In both cases the Reynolds numbers are much less than 1. The capillary pressure was determined to be the difference between gas and liquid pressures ($P_{cap} = P_g - P_l$) for both the inlet and outlet of the fracture.

4.1.1.2. Time Series Analysis

[67] For experiment A, periods of practically stable inlet and outlet gas and liquid pressures, shown in Figure 10a, are interrupted by bursts. *Persoff and Pruess* [1995] explained that instabilities in the liquid and air pressures resulted from recurring changes in phase occupancy between liquid and gas at a critical pore throat. Using a time series analysis, the Fourier transform plot exhibits broadband random fluctuations (Figure 10b), and the autocorrelation function exhibits cycling fluctuations (Figure 10c) caused by the pressure spikes. Hurst exponents of the inlet and outlet gas pressures are 0.1147 and 0.0996, respectively, implying a higher random component in the outlet time series data. Figure 10d shows a 2-D attractor (map) of normalized time intervals between bursts ($m = t_i/t_{max}$). The experimental data shown in Figure 10d by solid symbols can be described by a simple exponential equation, equation (16), with a small noise. Using this equation, we predicted the time intervals between bursts for two slightly different initial values of t_i, shown in Figure 10e. Figure 10e illustrates that a small difference in

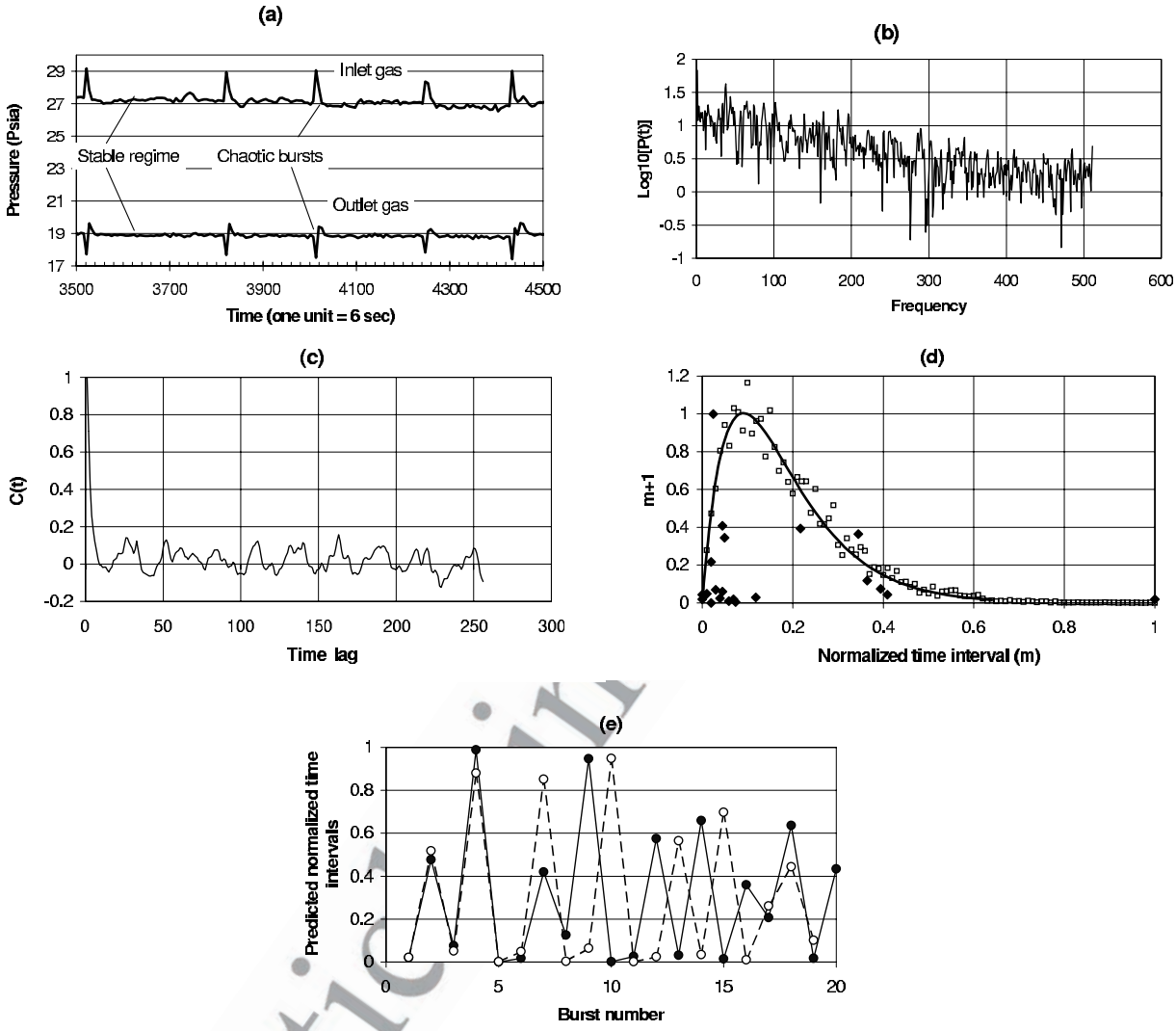

Figure 10. (a) Example of temporal variations of the inlet and outlet liquid and gas pressures at the inlet and outlet edges of the fracture replica, experiment *A* of *Persoff and Pruess* [1995], identifying periods of stable regime and chaotic bursts (note that 1 bar = 14.507 psi). (b) The fast Fourier transform plot. (c) The autocorrelation function. (d) An attractor (map) of the normalized time intervals between bursts ($m = t_i/t_{max}$) shown in Figure 10a, where solid symbols are experimental data, line is calculated from equation (16) with $A = 30$ and $\alpha = 11$, and open symbols are calculated with the same A and α and a random component of 10%. (e) Predicted normalized time intervals between bursts versus a burst number for two slightly different initial points: 0.0197 (solid line) and 0.022 (dashed line).

the initial value of t_i does not affect short-term predictions but causes a significant difference in predictions several steps (bursts) ahead, while the overall long-term range of time intervals between bursts remains the same.

[68] For experiment C, temporal variations of the capillary pressure exhibit quasiperiodic cycling with relatively short periods of laminar flow, which are interrupted by chaotic fluctuations, as shown in Figures 11a and 11b. The rapid drop of the capillary pressure at the end of each chaotic phase most likely indicates a liquid breakthrough at a pore throat [*Persoff and Pruess*, 1995]. However, the inlet and outlet cycling patterns are different. As shown in Figures 11a and 11b, the outlet capillary pressure exhibits a larger magnitude of fluctuations than that at the inlet, probably caused by a capillary barrier (pore throat) effect near the exit from the fracture and a longer duration of the laminar phase than that at the inlet. We can hypothesize that the observed quasiperiodic pressure oscillations at both inlet and outlet ends of the fracture result from a superposition of the forward and return pressure waves. Theoretically, the forward and return waves must decay in the direction of flow [*Rabinovich and Trubetskov*, 1994, p. 228], implying the dispersion of flow. Figures 11a and 11b illustrate that the main patterns of the time series data sets are preserved using a low-pass filter, suggesting that the noise is only a small component of the data. A graph showing the Fourier transformation of the time series data exhibits noisy-looking, broadband fluctuations (Figure 11c). An autocorrelation function indicates the phase-forgetting quasi-cycles (Figure 11d), consistent with the deterministic

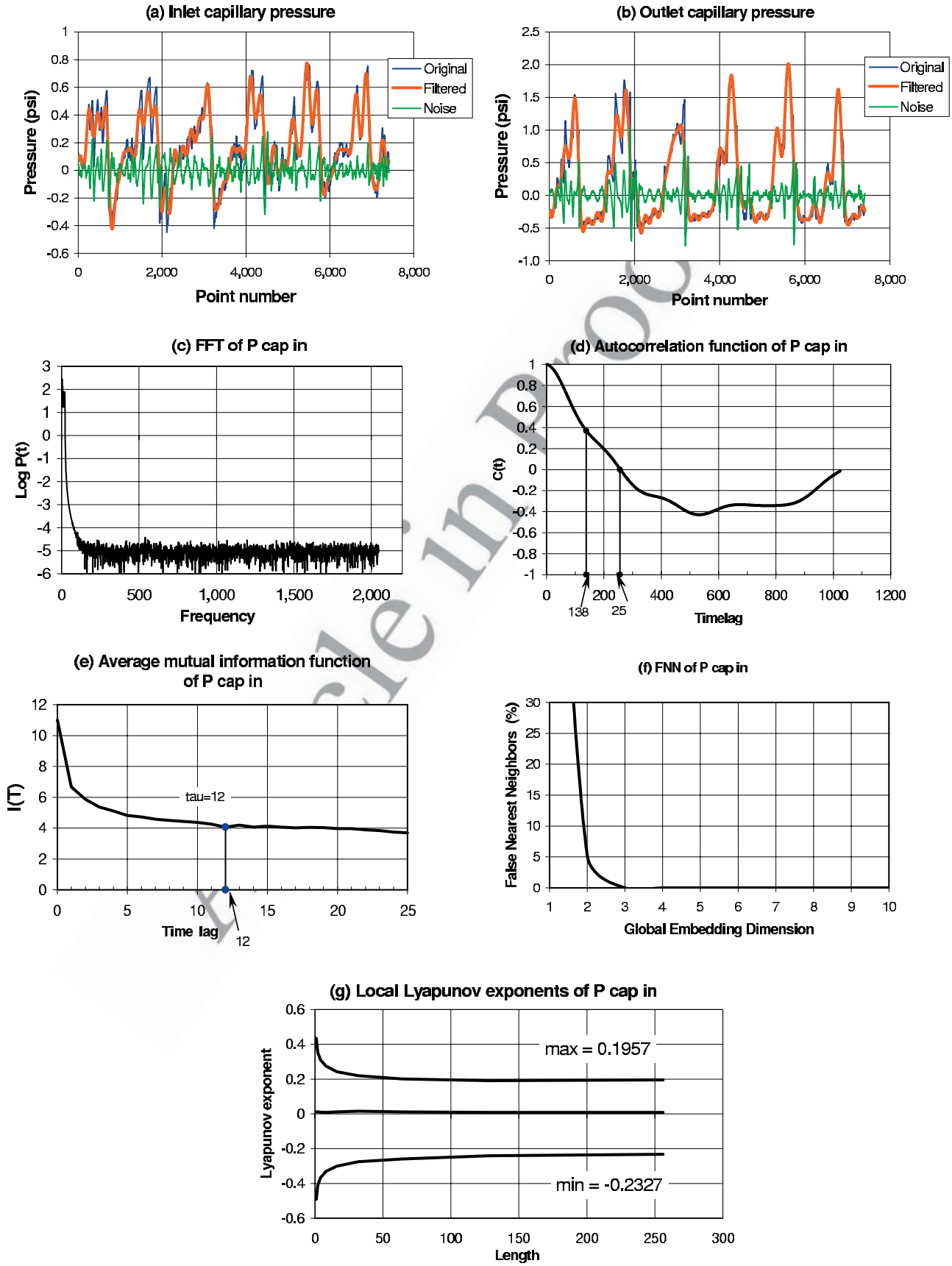
(a) Inlet capillary pressure
Pressure (psi)
Point number
Original
Filtered
Noise
(b) Outlet capillary pressure
Pressure (psi)
Point number
Original
Filtered
Noise
(c) FFT of P cap in
Log P(t)
Frequency
(d) Autocorrelation function of P cap in
C(t)
Timelag
138
25
(e) Average mutual information function of P cap in
I(T)
tau=12
Time lag
12
(f) FNN of P cap in
False Nearest Neighbors (%)
Global Embedding Dimension
(g) Local Lyapunov exponents of P cap in
Lyapunov exponent
max = 0.1957
min = -0.2327
Length

Figure 11

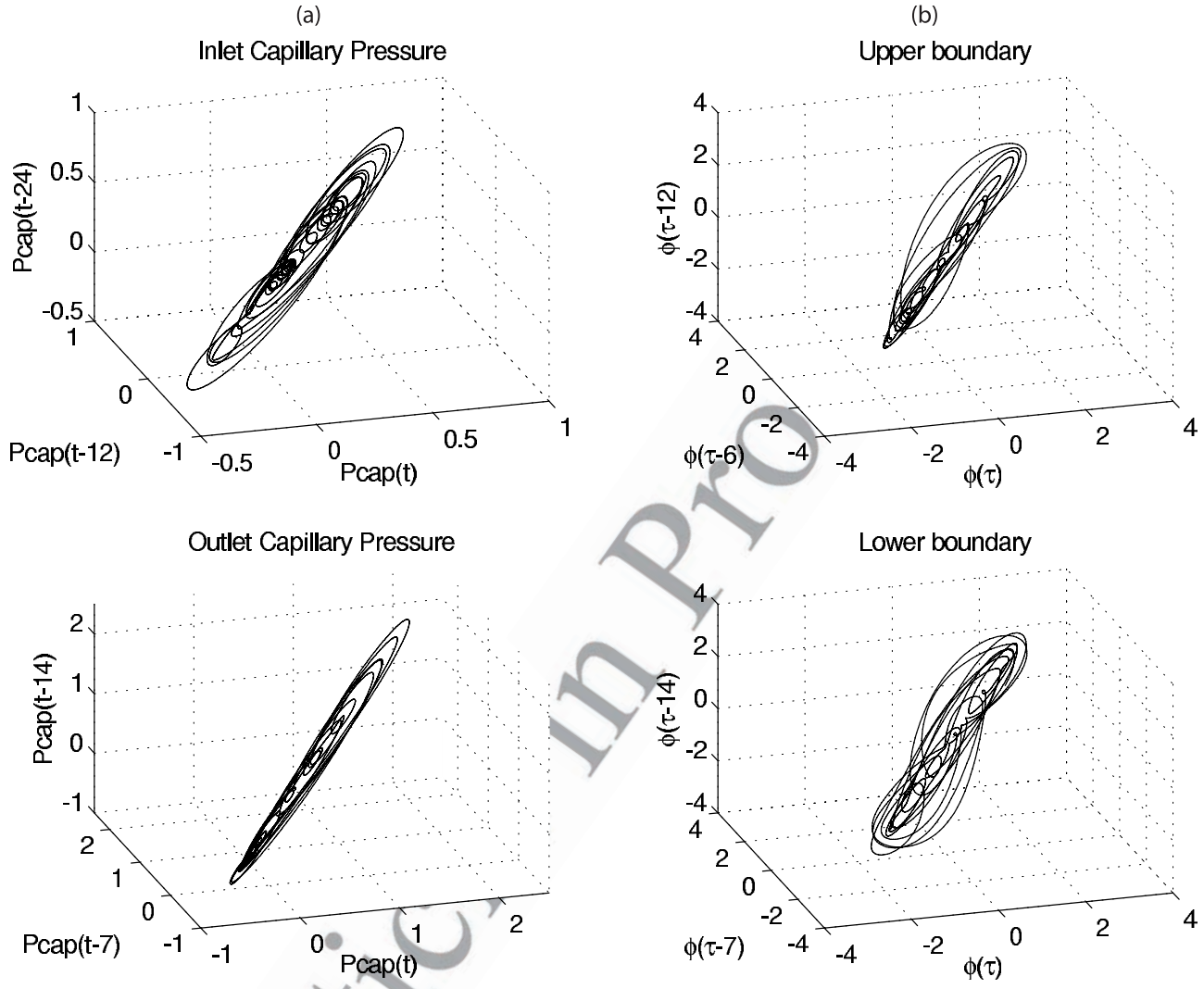

Figure 12. (a) Three-dimensional pseudo phase space attractors for the inlet and outlet capillary pressures. (b) Attractors of the Kuramoto-Sivashinsky equation (22).

chaotic process (see a discussion in section 2.2 and Figure 4) and a process of mixing [*Rabinovich and Trubetskov*, 1994]. The first local minimum of the average mutual information function (I) versus time lag (τ) occurs at $\tau = 12$ (Figure 11e), which is considered to be the time delay [*Abarbanel*, 1996]. The time delay $\tau = 12$ is then used to determine the embedding dimension of the phase space using the FNN method. The FNN plot reaches zero at $D_{GED} = 3$ (Figure 11f). For this data set, $D_L = 3$; therefore three local Lyapunov exponents were calculated, with the largest Lyapunov exponent being positive and the smallest Lyapunov exponent being negative (Figure 11g), which are typical for a deterministic chaotic system. Both the inlet (Figure 11g) and outlet capillary pressures produce a zero Lyapunov exponent, implying that the dynamic system (flow) can be described by a set of differential equations [*Abarbanel*, 1996]. The Lyapunov dimensions D_{Lyap} for the inlet and outlet capillary pressures are 2.849 and 2.422, respectively. The correlation dimensions, D_{cor}, for the inlet and outlet capillary pressures are 2.395 and 2.058, respectively. Note that the calculation results meet the inequality criterion $D_{Lyap} \geq D_{cor}$, typical for low-dimensional chaos [*Tsonis*, 1992]. According to equation (7), for $D_{GED} = 3$ the number of points needed to assess the correlation dimension should be at least 1585; we used a data set of 7410 points, so it should produce reliable calculation results.

[69] The remarkable feature of the pseudo phase space three-dimensional attractors for the inlet and outlet capillary pressures is that these attractors have definite structures (Figure 12a), and they are similar to the attractors of the

Figure 11. Temporal variations of (a) inlet and (b) outlet capillary pressures (black lines) calculated as the difference between the gas and liquid pressures (experiment C of *Persoff and Pruess* [1995] using Stripa natural rock under controlled gas-liquid volumetric flow ratio of 2) and filtered capillary pressures and noise. (c) Fast Fourier transformation (FFT) of the time series data. (d) An autocorrelation function. (e) Average mutual information function versus the time lag, showing the first microminimum at $\tau = 12$. (f) The false nearest neighbors (FNN) plot, showing that the FNN reaches zero at $D_{GED} = 3$. (g) Local Lyapunov exponents.

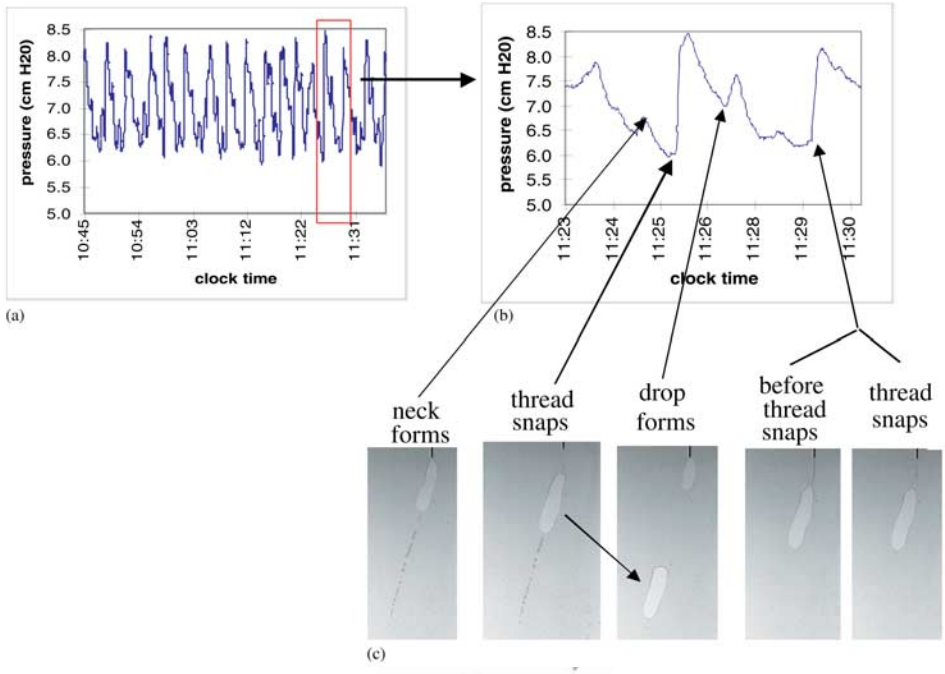

Figure 13. Correspondence between pressure time trend (at the entrance to the fracture model) and drip behavior (an experiment with the flow rate of 0.25 mL/h and needle point source within smooth glass plates separated by 0.36 mm shim): (a) pressure data, (b) expansion of the boxed section shown in Figure 13a, and (c) frames from video tape recording of experiment showing drip behavior [*Geller et al.*, 2001].

solution of the K-S equation shown in Figure 12b. This similarity implies that the fracture flow process can be described using the K-S equation (22).

4.1.2. Dripping-Water Experiments

4.1.2.1. Design of Experiments

[70] A series of laboratory experiments were conducted in which water was injected at a constant flow rate (from 0.25 to 20 mL/h) into fracture models (smooth, parallel glass plates separated by 350 μm and textured glass plates, inclined 60° from the horizontal) through a single capillary tube that terminated at the entrance to the fracture model [*Geller et al.*, 2001]. (In these experiments we also investigated the effects of the size and material of the capillary tube and the type of contact between the capillary tube and fracture model.) Liquid pressure was monitored upstream of the entrance to the fracture. It was observed that water seeped through the fracture models in discrete channels that undergo cycles of snapping and reforming, and liquid drips detached at different points along the water channel. Pressure fluctuations upgradient of the pressure sensor (Figure 13a) could be correlated to the growth and detachment of drips in the interior of the fracture observed directly and recorded with a video camera (Figure 13b).

4.1.2.2. Time Series Analysis

[71] Analysis of diagnostic parameters of chaos for these water-dripping experiments shows that all data sets contain a chaotic component. The local embedding dimensions (D_L) ranged from 3 to 10, with global embedding dimensions (D_{GED}) one to two units higher. The higher dimensionality of some of the data sets indicates either the presence of high-dimensional chaos or a significant random component. It was also determined that the injection flow rate affects seepage behavior in a fracture. As flow rate increases, the Hurst exponent linearly decreases, supporting the hypothesis that seepage becomes more random as flow rate increases. However, no simple, consistent correlations were determined between other diagnostic parameters of chaos and experimental variables. Three-dimensional pseudo phase space attractors exhibit definite structures, with some scattering of data points on the attractor confirming that flow behavior is mostly characterized by low-dimensional chaotic dynamics with some random components. To demonstrate a general trend of pressure fluctuations during the water injection through a capillary into a fracture replica, Figure 14a shows raw data (black line) and a noise-reduced curve (red line) for time variations of pressure. These data were collected at time intervals of 1.1 s using a rough-walled (glass plate) fracture model in an experiment with water supplied through a capillary tube 0.8 mm in diameter under a constant flow rate of 10 mL/h. The 3-D attractor of the raw pressure measurements (Figure 14b) shows a high concentration of points along directions of axes, which was most likely caused by noise. (Such behavior was observed in laboratory experiments of water droplet avalanches by *Plourde and Bretz* [1993].) The 3-D attractor of noise-reduced data (Figure 14c) is geometrically similar to that of the solution of the K-S equation for film flow (see Figure 12b). Thus we can conjecture that a combined process of intrafracture water film flow and water dripping

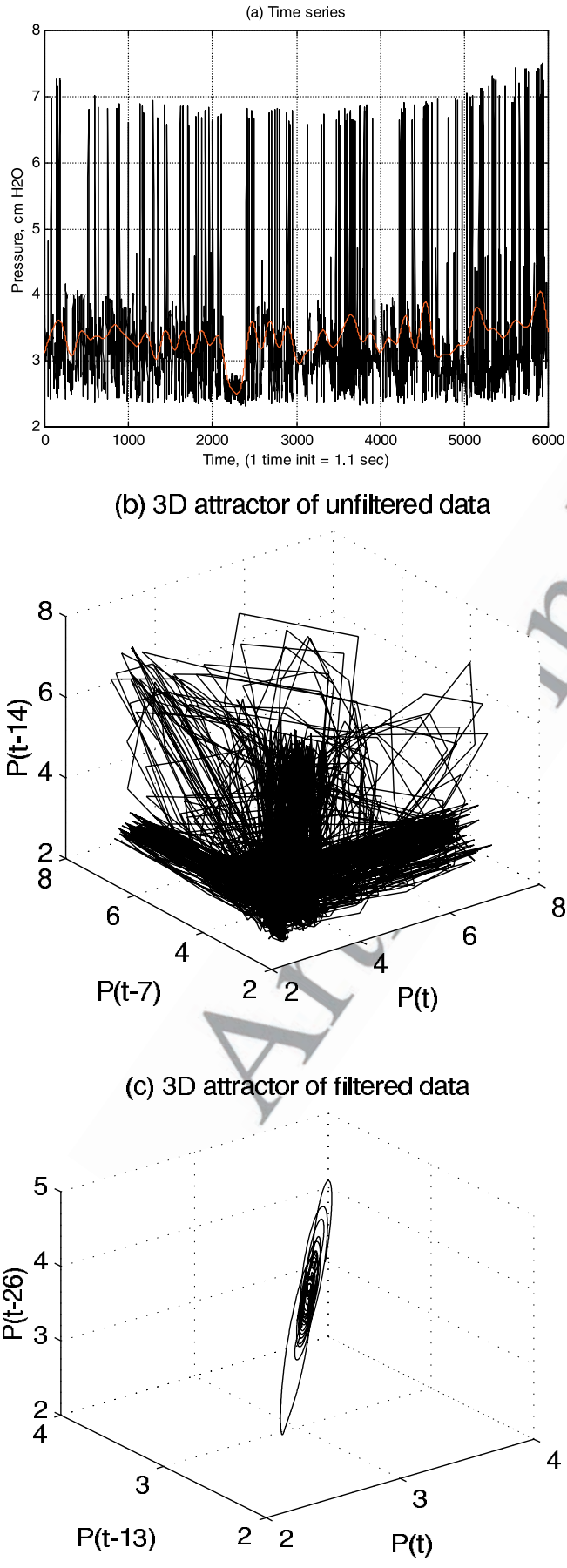

in a partially saturated fracture is characterized by both deterministic chaotic and random components.

4.2. Field Infiltration Tests to Characterize Unstable Infiltration in Unsaturated Fractured Rock

[72] In analyzing the results of field infiltration tests in fractured rock we must assess the effect of infiltration, occurring at the surface; intrinsic fracture (intrafracture) seepage and dripping, occurring within a fracture plane; extrinsic fracture seepage (dripping water phenomena), occurring at the intersection of a fracture with a rock cavity or another fracture; and fracture-matrix interaction, resulting in matrix imbibition. It is a challenging problem to distinguish between these processes, because fracture flow processes cannot be measured directly under field conditions; monitoring probes are not inserted directly into fractures and provide only volume-averaged values of flow parameters characterizing both the matrix and fractures. Therefore the main point of our analysis in section 4.2.1 is to distinguish chaos generated by dripping from a fracture (associated with a capillary barrier effect) from the effects of intrafracture flow and thus to determine if the intrafracture flow is by itself chaotic. In section 4.2.2 we will discuss the results of an analysis of the time variations of the infiltration rate and the measurements of intersecting flow paths in fractured rock, indicating a possibility of chaotic behavior.

4.2.1. Basalt at the Hell's Half Acre Field Site

[73] Several small-scale ponded infiltration tests were conducted in fractured basalt in 1998–1999 at the Hell's Half Acre (HHA) field site (near INEEL, Idaho) using a small reservoir (40 × 80 cm) constructed on the surface exposure of a fracture at an overhanging basalt ledge [*Podgorney et al.*, 2000]. The ponded infiltration tests included measurements of reservoir water head, flow into the reservoir (used to estimate infiltration rate), flow into a grid of pans beneath the overhanging ledge (used to estimate outflow rate), capillary pressure and temperature in the rock matrix and fractures, ambient temperature and barometric pressure, and temporal and spatial monitoring of dripping water (up to millions of data points) from the undersurface of the ledge. It was determined that despite the constant head ponded water level, infiltration rate exhibited a general three-stage trend of temporal variations (identical to those observed during the infiltration tests in soils in the presence of entrapped air and described in section 3.2), accompanied by high-frequency oscillations (Figure 15a). We assume that high-frequency fluctuations are mostly generated by dripping from a fracture, while low-frequency fluctuations are mostly generated by intrafracture flow. To better understand the physics of these

Figure 14. Results of analysis of pressure measurements conducted in a rough-walled fracture model with a flow rate of 10 mL/h supplied through a capillary tube. (a) Time trend of pressure measured at the entrance to the capillary tube. Black line is raw data, and red line is a low-pass-filtered data. (b) The 3-D attractor of raw data. (c) Attractor of the low-pass-filtered data.

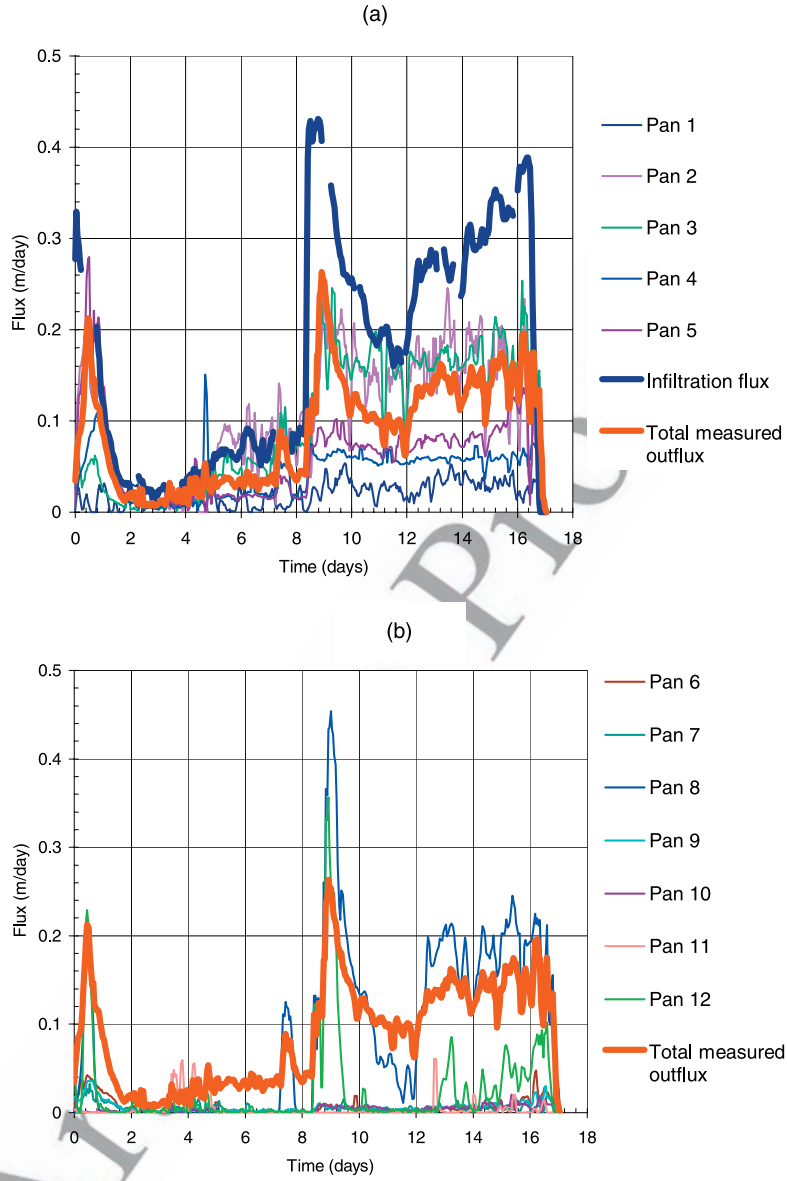

Figure 15. (a) Infiltration and total seepage rates and seepage collected by individual pans located beneath the infiltration gallery. (b) Seepage rate collected by pans located outside the infiltration gallery at the Hell's Half Acre (HHA) site, test 8, 1998. (c) Comparison of 3-D attractors for the infiltration and seepage rates (noise-reduced data) at HHA site, test 8, 1998.

processes, we provided a phase space reconstruction of the infiltration and outflow rates and determined diagnostic parameters of chaos for dripping intervals. Analysis of the infiltration and outflow rates (noise-reduced trends) indicates almost similar 3-D attractors of spiral shapes with a few saddle points (Figure 15b), implying a possibility of a deterministic chaotic process. Analysis of water-dripping intervals reveals that water-dripping behavior at the fracture exit was unstable and irregular in space and time [*Podgorney et al.*, 2000].

[74] To demonstrate that dripping behavior is nonstationary and exhibits different types of chaos over time, Figures 16a–16e present time series of drip intervals versus the drip number, and Figure 16f shows corresponding 2-D attractors for one of the dripping points at the HHA site. The beginning of the test is characterized by quasiperiodic, almost double-cycling fluctuations around a constant mean value (Figure 16a, points 1–500), with the attractor typical for a quasiperiodic regime (Figure 16f). The following slight increase in the mean value (Figure 16b, points 500–1100) results in a shift in the attractor. While the increase in the mean dripping interval persists, starting from approximately point 900 (Figure 16b), the magnitude of fluctuations gradually dies out (Figure 16c, points 1150–2500). The next segment (Figure 16d, points 2500–4400) represents a gradual increase in the periodicity of fluctuations, followed by quasiperiodic fluctuations (Figure 16e). The most interesting observation is the change in the shape

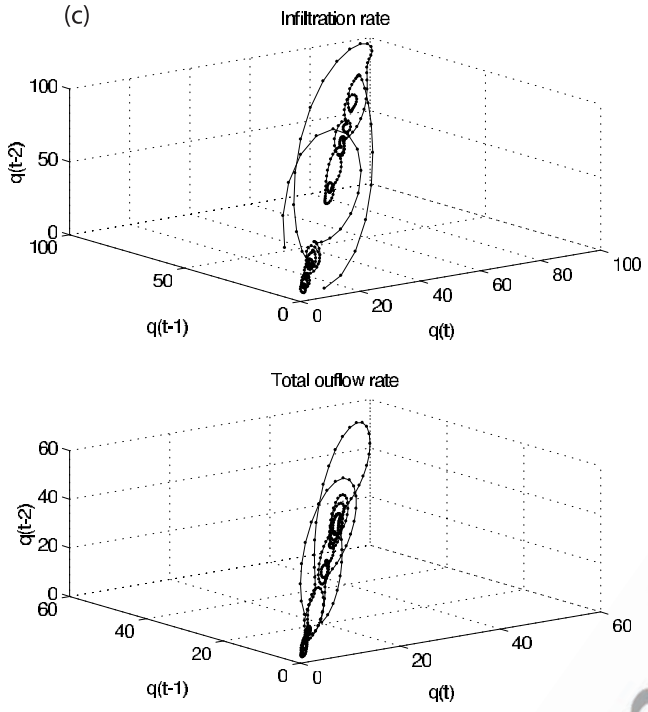

Figure 15. (continued)

of the attractor, which becomes reversed compared to that at the beginning of the test.

[75] Time series of water-dripping intervals reflects generally both the intrafracture flow processes (low-frequency fluctuations) and dripping itself (high-frequency fluctuations) generated at the fracture-air interface [*Faybishenko*, 2002]. The low-frequency fluctuations (that are assumed to represent intrafracture flow) are described by attractors similar to those for the laboratory partially saturated fracture flow experiments and the Kuramoto-Sivashinsky equation (see section 4.1). This similarity would support the notion that intrafracture flow is deterministic chaotic, with a certain random component.

4.2.2. Other Examples of Flow Instability

4.2.2.1. Yucca Mountain Infiltration Tests in Fractured Tuff

[76] A series of infiltration tests were conducted at Yucca Mountain to assess hydraulic processes in fractured tuff. The time variations of the infiltration rate (Figure 17a), which were measured during an infiltration test conducted at alcove 6 of Yucca Mountain [*Salve et al.*, 2002], were used to plot a phase plane diagram as the relationship between dq/dt and q. Figure 17a shows two groups of points based on the rate of changing the infiltration rate: (1) slow motion points within an oval, representing slowly changing flow rate fluctuations, and (2) fast motion along the curves (drawn schematically), converging to the oval and representing rapidly changing flow rate fluctuations. Such attractors, which are common in describing nonlinear physical processes, are also typical for pulsation and relaxation oscillations [*Rabinovich et al.*, 2000]. Infiltration tests in fractured tuff show that the nonlinear dynamics of extrinsic seepage and gravity drainage processes depend on several factors, such as multiple intrafracture threshold effects caused by fracture asperities, matrix imbibition, and, possibly, a capillary barrier effect at the water outlet [*Faybishenko et al.*, 2003b]. Moreover, it was determined that the attractors for the infiltration and extrinsic rates are different, suggesting that different dynamic effects are involved in fracture seepage near the entrance and exit from the fracture.

4.2.2.2. Infiltration Tests in Unsaturated Fractured Chalk in the Negev Desert

[77] *Dahan et al.* [2001] studied flow and transport in the unsaturated fractured chalk of the Negev desert, using ponded infiltration tests with tracers (tritium, oxygen 18, deuterium, chloride, and bromide). They suggested that over 70% of the water was transmitted through less than 20% of the fractures. The flow rate changed drastically over the ponding area, with both abrupt and gradual temporal and spatial variations (Figure 18a). An important result of this test is that flow trajectories connecting the surface pond with the receiving samplers are likely to intersect each other, which is shown in Figure 18b. Moreover, flow trajectories are dynamic and not precisely repeated in the different tests at this site.

4.2.2.3. Infiltration Tests in Unsaturated Fractured Basalt in Idaho

[78] A series of infiltration tests at the Box Canyon site in Idaho showed that under virtually the same water level in the infiltration pond, flow paths in the underlying fractured basalt varied and created (presumably) intersecting flow paths [*Faybishenko et al.*, 2000], further evidence of chaos. Experimental results [*Faybishenko et al.*, 2000, 2001b] and numerical modeling [*Doughty*, 2000] of the infiltration tests (with a constant head and tracer concentration boundary) at Box Canyon and large-scale infiltration tests show a variety of the tracer breakthrough curves (BTCs), including multimodal curves produced by migration from different fractures. At some points, no tracer is detected, possibly because initial (untraced) water may flow into dead-end, nonconductive fractures easily, but it cannot continue flowing out of these fractures, so no subsequent tracer can flow into these fractures by advection. Tracer can enter saturated or nonconductive fractures only by diffusion, which is a relatively slow process. It is important to indicate that BTCs do not correlate with the depth or lithology of the monitoring points. Rather, the BTCs are dependent on the overall geometry of the fracture pattern, including the fractures above and below the monitoring location.

5. CONCLUDING REMARKS AND PERSPECTIVES

[79] Instability and complexity of flow and transport processes in partially saturated, heterogeneous soils and fractured rock are induced by two key elements: (1) complex geometry of preferential flow paths (as affected by rock discontinuity and heterogeneity on all scales, from a rough fracture surface to an irregular fracture network) and (2) nonlinear dynamic processes such as episodic and preferential flow, funneling and divergence of flow paths, transient flow behavior, nonlinearity, film flow along frac-

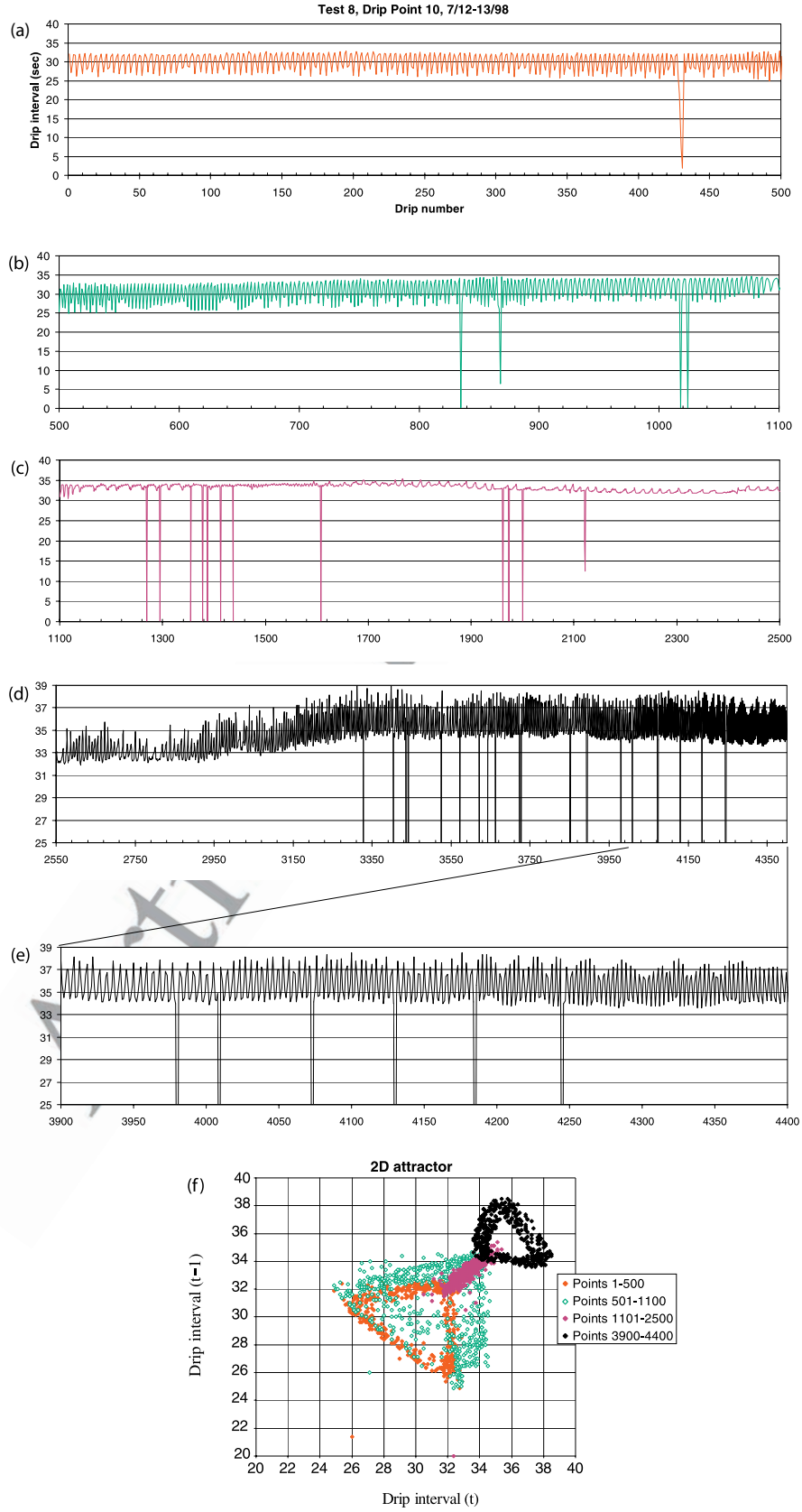
Test 8, Drip Point 10, 7/12-13/98
(a)
Drip interval (sec)
Drip number
(b)
(c)
(d)
(e)
(f)
2D attractor
Drip interval (t-1)
Drip interval (t)
Points 1-500
Points 501-1100
Points 1101-2500
Points 3900-4400

Figure 16

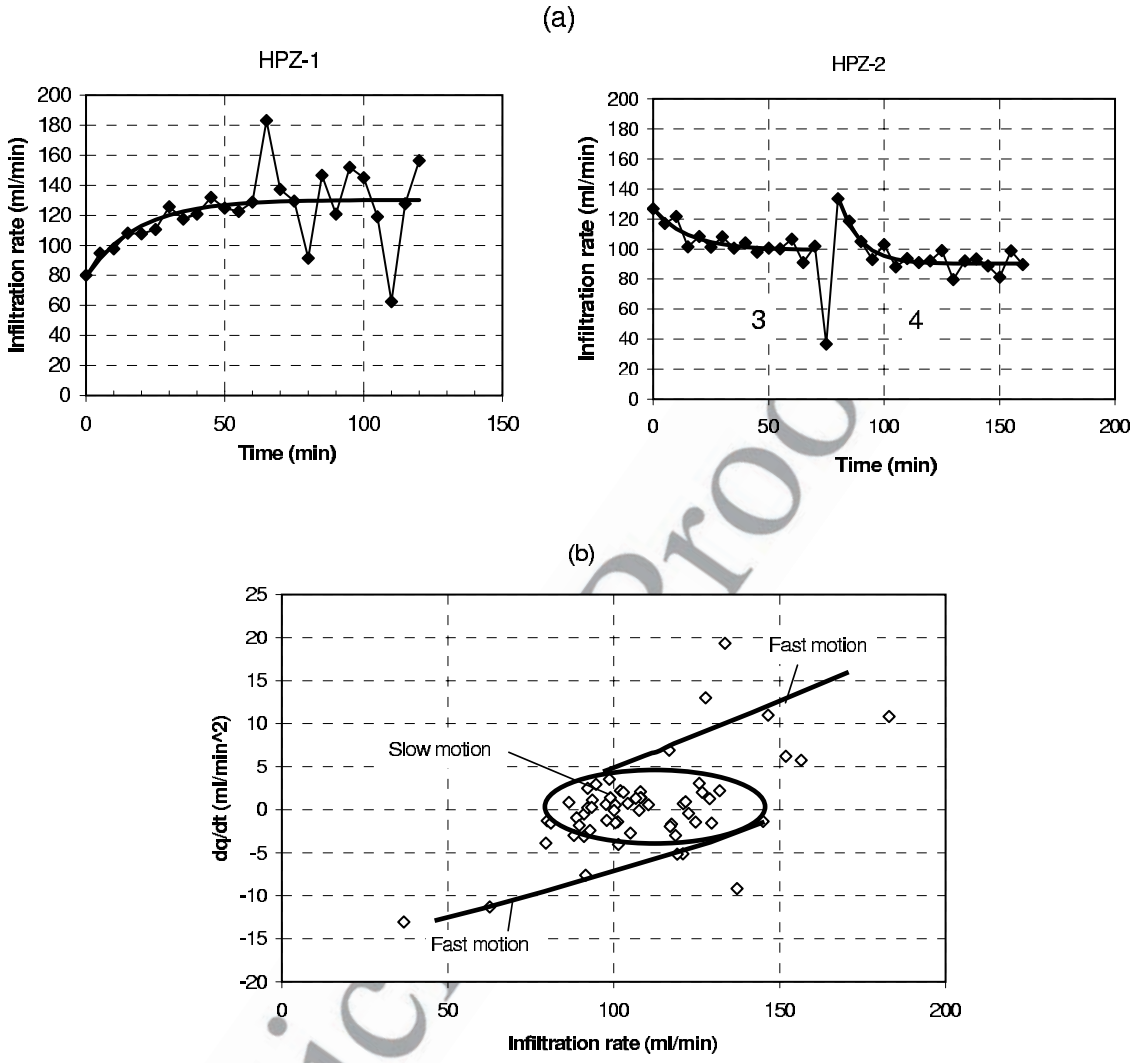

Figure 17. (a) The time variations of the infiltration rate measured during the infiltration test at alcove 6 of Yucca Mountain [*Salve et al.*, 2002] and (b) corresponding the phase plane diagram as the relationship between dq/dt and q [*Faybishenko*, 2002].

ture surfaces, intrafracture water dripping, entrapped air, fracture-matrix interaction, and pore throat effects. The superposition, feedback, and competition of these physical processes create a nonlinear dynamic system, generating a deterministic chaotic behavior with a random component.

[80] Our analysis shows that vadose zone processes meet the criteria of a nonlinear dynamic system, as the unsaturated flow processes are nonlinear, sensitive to initial conditions, and generated by intrinsic properties of the system (not random external factors) and are not governed by Darcy's law at a local scale during the periods of chaotic fluctuations. Chaotic fluctuations for water pressure, flow rate, and water dripping on different timescales have been observed in laboratory and field experiments.

[81] For deterministic chaotic, intrafracture flow processes the models of chaos theory can be used for accurate short-term predictions of system behavior, but conventional stochastic models could be used for long-term predictions. Furthermore, deterministic chaos, in conjunction with system noise and errors of measurements, creates a source of irreducible uncertainty for long-term predictions. Therefore the predictability of a vadose zone system cannot be signif-

Figure 16. (a)–(e) Time series and (f) attractors of dripping intervals for dripping point 10 (HHA infiltration test 8, 1999), demonstrating different types of chaos developed over time with a corresponding shift in the attractor. Figure 16a shows points 1–500, quasiperiodic, almost double-cycling fluctuations around a constant mean value Figure 16b shows points 501–1100; the amount of noise increases and the attractor is shifted. Figure 16c shows points 1101–2500; the fluctuations gradually die out and the attractor becomes a group of minor noisy fluctuations. Figure 16d shows points 2550–43500, a gradual increase in the periodicity of fluctuations, while the attractor is inverted compared to that for points 1–500. Figure 16e shows an expanded view of the portion of Figure 16d between drips 3900 and 4400. Figure 16f shows the 2-D attractor, demonstrating the shift in the attractor' shape over time.

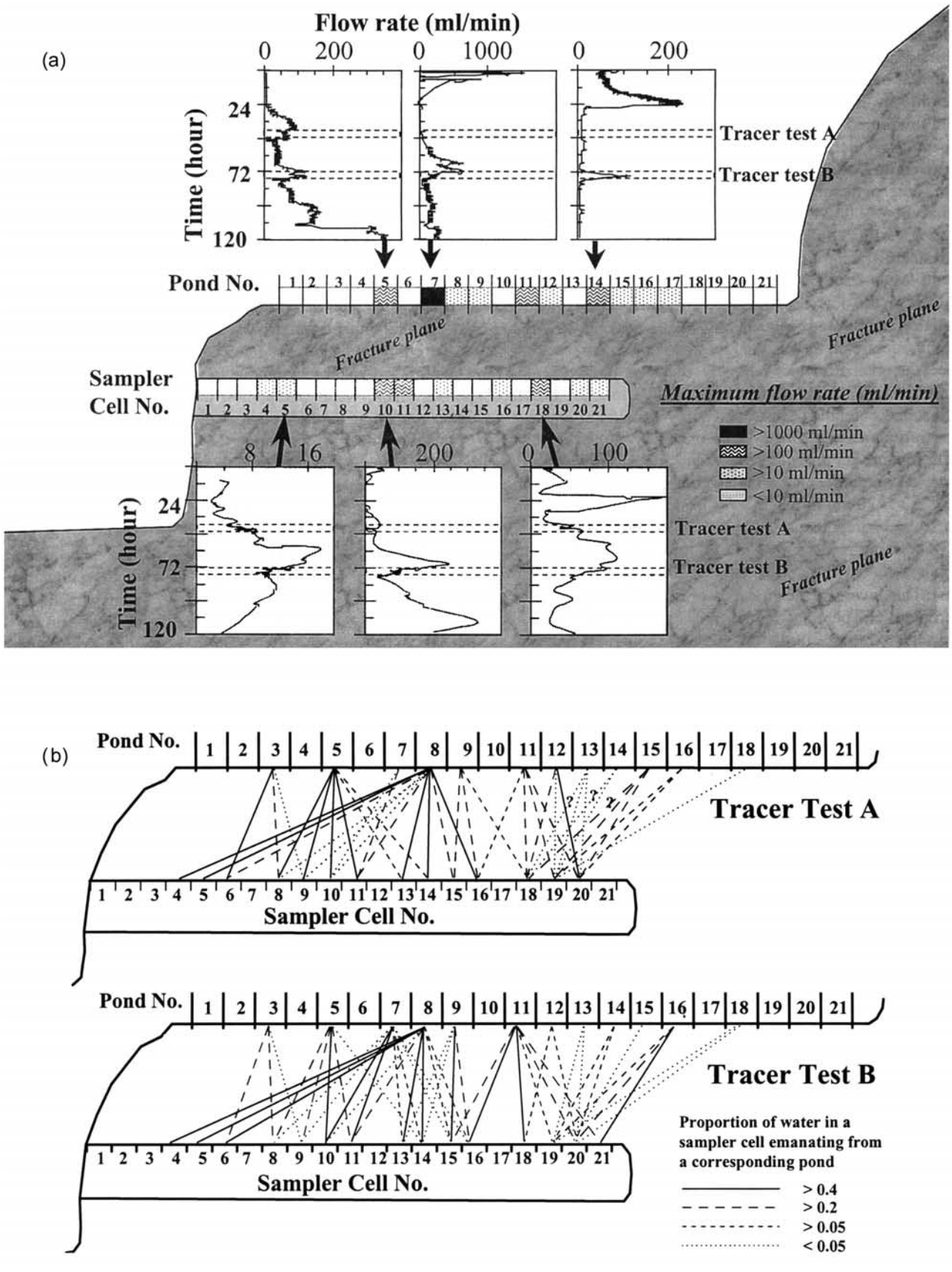

Figure 18. Design and the results of the ponded infiltration test in unsaturated fractured chalk in the Negev desert [*Dahan et al.*, 2001], showing (a) the temporal variations of the flow rate, exhibiting both abrupt and gradual variations, and (b) intersecting flow trajectories connecting the pond with the water samplers.

icantly improved by making more precise measurements of initial and boundary conditions and system parameters. The use of nonlinear dynamic methods is expected to improve our understanding of limitations on the accuracy of predicting hydraulic behavior in unsaturated media using conventional volume-averaged Darcy's law and Richards' equation. As time series data are more easily obtained from field observations, these parameters can then be used to assess the spatial variation of flow processes in the subsurface, which are difficult, if not impossible, to measure directly.

[82] Challenging theoretical and practical problems remain to be studied. For example, we should consider systems with multiple timescales, which may create the complex dynamics of high-dimensional state spaces arising in fracture flow processes. The remaining question is how the knowledge of nonlinear dynamics discovered in many theoretical, laboratory and small-scale field studies can be used to understand large-scale field phenomena. Other formidable practical problems would involve using theory of the chaotic processes of chemical diffusion and mixing in designing remediation schemes for contaminated sites or the effect of heat and mass transfer at the nuclear waste disposal sites. The use of nonlinear dynamics could significantly improve solutions of many practical problems, for instance, predictions of unsaturated flow and dripping water into underground openings such as caves [*Genty and Deflandre*, 1998; *Or and Ghezzehei*, 2000] and a tunnel at the potential nuclear waste repository at Yucca Mountain, remediation of contaminated unsaturated rocks, and climate predictions.

[83] The significance of using nonlinear dynamics in earth sciences disciplines is difficult to overestimate, because we now collect a tremendous amount of data characterizing a variety of temporal and spatial subsurface processes. Although nonlinear dynamics models could be considered as an alternative to the conventional statistical approach, they are basic to the characterization of physical phenomena encountered in unsteady hydrologic processes. However, these models are at an early stage of development. Describing complex, nonlinear geophysical systems will be one of the greatest challenges facing scientists working in different fields of earth sciences well into the 21st century.

[84] **ACKNOWLEDGMENTS.** Reviews by Chris Doughty and Dan Hawkes of LBNL, Bob Glass of Sandia Labs, and two anonymous reviewers are very much appreciated. The author is thankful to colleagues at LBNL (Jil Geller and Sharon Borglin) and INEEL (Tom Wood and Robert Podgorney), who participated in field and laboratory investigations discussed in this paper. This work was partially supported by the Director, Office of Science, Office of Basic Energy Sciences, the Environmental Management Science Program of the U.S. Department of Energy under contract DE-AC03-76SF00098.

[85] Daniel Tartakovsky was the Editor responsible for this paper. He thanks two technical reviewers and one cross-disciplinary reviewer.

REFERENCES

Abarbanel, H. D. I. (1996), *Analysis of Observed Chaotic Data*, Springer-Verlag, New York.

Abarbanel, H. D. I., and L. S. Tsimring (1998), Reader's guide to toolkit for nonlinear signal analysis, manual, Univ. of Calif., San Diego.

Abraham, R. H., L. Gardini, and C. Mira (1997), *Chaos in Discrete Dynamical Systems*, Springer-Verlag, New York.

Acheson, D. (1997), *From Calculus to Chaos: An Introduction to Dynamics*, Oxford Univ. Press, New York.

Ambravaneswaran, B., S. D. Phillips, and O. A. Basaran (2000), Theoretical analysis of a dripping faucet, *Phys. Rev. Lett.*, *85*, 5332–5335.

Arnold, V. I. (1984), *Catastrophe Theory*, Springer-Verlag, New York.

Baas, N. A., and C. Emmeche (1997), On emergence and explanation, *Intellectica*, *2*(25), 67–83.

Babchin, A. J., A. L. Frenkel, B. G. Levich, and G. I. Sivashinsky (1983), Flow-induced nonlinear effect in thin film stability, *Ann. N. Y. Acad. Sci.*, *404*, 426 pp.

Baker, G. L., and J. P. Gollub (1996), *Chaotic Dynamics: An Introduction*, Cambridge Univ. Press, New York.

Barenblatt, G. I., T. W. Patzek, and D. B. Silin (2002), The mathematical model of non-equilibrium effects in water-oil displacement, Paper SPE 75169 presented at SPE/DOE Thirteenth Symposium on Improved Oil Recovery, Soc. of Pet. Eng., Tulsa, Okla., 13–17 April.

Barton, C. C., and E. Larsen (1985), Fractal geometry of two-dimensional fracture networks at Yucca Mountain, southwest Nevada, in *Fundamentals of Rock Joints: International Symposium on Fundamentals of Rock Joints*, edited by O. Stephansson, pp. 74–84, Centek, Lulea, Sweden.

Blitz, D. (1992), *Emergent Evolution*, Kluwer Acad., Norwell, Mass.

Bour, O., and P. Davy (1997), Connectivity of random fault networks following a power law fault length distribution, *Water Resour. Res.*, *33*(7), 1567–1583.

Cahill, A. T., and M. B. Parlange (1998), On water vapor transport in field soils, *Water Resour. Res.*, *34*(4), 731–739.

Carr, J. R. (1989), Fractal characterization of and joint surface roughness in welded tuff at Yucca Mountain, Nevada, in *Proceedings of the Thirtieth U.S. Symposium Rock Mechanics, Morgantown, West Virginia*, edited by A. W. Khair, pp. 193–200, A. A. Balkema, Brookfield, Vt.

Chaté, H., A. Lemaître, P. Marcq, and P. Manneville (1996), Nontrivial collective behavior in extensively-chaotic dynamical systems: An update, *Physica A*, *224*, 447–457.

Cheng, Z., S. Redner, P. Meakin, and F. Family (1989), Avalanche dynamics in a deposition model with "sliding," *Phys. Rev. A*, *40*(10), 5922–5935.

Conca, J. L., and J. Wright (1994), The UFATM technology for characterization of in situ barrier materials, in *In Situ Remediation: Scientific Basis for Current and Future Technologies*, pp. 1179–1194, Battelle, Columbus, Ohio.

Crawford, J., P. Baveye, P. Grindrod, and C. Rappoldt (1999), Application of fractals to soil properties, landscape patterns and solute transport in porous media, in *Assessment of Non-Point Source Pollution in the Vadose Zone*, edited by D. L. Corwin, K. Loague, and T. R. Ellsworth, *Geophys. Monogr. Ser.*, vol. 108, pp. 151–164, AGU, Washington, D. C.

Cunningham, A. B. (1993), Influence of biofilm accumulation on porous media hydrodynamic properties, in *Manipulation of Groundwater Colloids for Environmental Restoration*, edited by J. F. McCarthy and F. J. Wobber, pp. 103–109, Lewis, Boca Raton, Fla.

da Cunha, A. P. (Ed.) (1993), Scale effects in rock masses, in *Proceedings of the Second International Workshop on Scale Effects in Rock Masses*, A. A. Balkema, Brookfield, Vt.

Dahan, O., R. Nativ, E. M. Adar, and B. Berkowitz (2001), Water flow and solute transport in unsaturated fractured chalk, in *Flow and Transport Through Unsaturated Fractured Rock*, 2nd ed.,

Geophys. Monogr. Ser., vol. 42, edited by D. D. Evans, T. J. Nicholson, and T. C. Rasmussen, pp. 183–196, AGU, Washington, D. C.

Deriagin, B. V., N. V. Churaev, and V. M. Muller (1985), *Surface Forces* (in Russian), Nauka, Moscow.

Deriagin, B. V., Z. M. Zorin, and N. V. Churaev (1989), Water films on solid hydrophilic surfaces, in *Water in Disperse Systems* (in Russian), pp. 210–228, Chemistry, Moscow.

Dewers, T., and P. Ortoleva (1994), Nonlinear dynamical aspects of deep basin hydrology—Fluid compartment formation and episodic fluid release, *Am. J. Sci.*, *294*(6), 713–755.

Doughty, C. (2000), Numerical model of water flow in a fractured basalt vadose zone, Box Canyon site, Idaho, *Water Resour. Res.*, *36*(12), 3521–3534.

Doughty, C., and K. Karasaki (2002), Flow and transport in hierarchically fractured rock, *J. Hydrol.*, *263*, 1–22.

Dubois, J. (1998), *Non-Linear Dynamics in Geophysics*, John Wiley, Hoboken, N. J.

Dykhuizen, R. C. (1992), Diffusive matrix fracture coupling including the effects of flow channeling, *Water Resour. Res.*, *28*(9), 2447–2450.

Entekhabi, D., I. Rodriguez-Iturbe, and F. Castelli (1996), Mutual interaction of soil moisture state and atmospheric processes, *J. Hydrol.*, *184*, 3–17.

Faybishenko, B. A. (1995), Hydraulic behavior of quasi-saturated soils in the presence of entrapped air: Laboratory investigations, *Water Resour. Res.*, *31*(10), 2421–2436.

Faybishenko, B. (1999), Comparison of laboratory and field methods for determination of unsaturated hydraulic conductivity of soils, in *Proceedings of the International Workshop on Characterization and Measurement of the Hydraulic Properties of Unsaturated Porous Media*, edited by M. T. van Genuchten et al., pp. 279–292, Univ. of Calif., Riverside.

Faybishenko, B. (2002), Chaotic dynamics in flow through unsaturated fractured media, *Adv. Water Resour.*, *25*, 793–816.

Faybishenko, B., and S. Finsterle (2000), Tensiometry in fractured rocks, in *Theory, Modeling, and Field Investigation in Hydrogeology: A Special Volume in Honor of Shlomo P. Neuman's 60th Birthday*, edited by D. Zhang and C. L. Winter, *Spec. Pap. Geol. Soc. Am.*, *348*, 161–174.

Faybishenko, B., C. Doughty, M. Steiger, J. C. S. Long, T. R. Wood, J. S. Jacobsen, J. Lore, and P. T. Zawislanski (2000), Conceptual model of the geometry and physics of water flow in a fractured basalt vadose zone, *Water Resour. Res.*, *36*(12), 3499–3520.

Faybishenko, B., P. A. Witherspoon, C. Doughty, J. Geller, T. Wood, and R. Podgorney (2001a), Multi-scale investigations of liquid flow in a fractured basalt vadose zone, in *Flow and Transport Through Unsaturated Fractured Rock*, *Geophys. Monogr. Ser.*, vol. 42, 2nd ed., edited by D. D. Evans, T. J. Nicholson, and T. C. Rasmussen, pp. 161–182, AGU, Washington, D. C.

Faybishenko, B., A. J. Babchin, A. L. Frenkel, D. Halpern, and G. I. Sivashinsky (2001b), A model of chaotic evolution of an ultrathin liquid film flowing down an inclined plane, *Colloids Surf. A*, *192*(1–3), 377–385.

Faybishenko, B., G. S. Bodvarsson, J. Hinds, and P. A. Witherspoon (2003a), Scaling and hierarchy of models for flow processes in unsaturated fractured rock, in *Scaling Methods in Soil Physics*, edited by Y. A. Pachepsky, D. E. Radcliffe, and H. M. Selim, pp. 373–417, CRC Press, Boca Raton, Fla.

Faybishenko, B., G. S. Bodvarsson, and R. Salve (2003b), On the physics of unstable infiltration, seepage, and gravity drainage in partially saturated tuffs, *J. Contam. Hydrol.*, *62–63*, 63–87.

Feder, J., and T. Jøssang (1995), Fractal patterns in porous media, in *Fractals in Petroleum Geology and Earth Processes*, edited by C. C. Barton and P. R. La Pointe, pp. 179–226, Plenum, New York.

Feldman, G. M. (1988), *Water Movement in Thawing and Freezing Soils*, Nauka, Novosibirsk, Moscow.

Flühler, H., A. J. Peck, and L. H. Stolzy (1986), Air pressure measurements, in *Methods of Soil Analysis, Part 1, Physical and Mineralogical Methods*, edited by A. Klute, *Soil Sci. Soc. Am. Book Ser.*, *5*, 1161–1172.

Freeze, R. A., and J. A. Cherry (1979), *Groundwater*, Prentice-Hall, Englewood Cliffs, N. J.

Frenkel, A. L., and K. Indireshkumar (1996), Derivations and simulations of evolution equations of wavy film flows, in *Mathematical Modeling and Simulation in Hydrodynamic Stability*, edited by D. N. Riahi, pp. 35–81, World Sci., River Edge, N. J.

Frenkel, A. L., A. J. Babchin, B. Levich, T. Shlang, and G. I. Sivashinsky (1987), Annular flows can keep unstable films from breakup: Nonlinear saturation of capillary instability, *J. Colloid Interface Sci.*, *115*, 225–233.

Fuentes, N. O., and B. Faybishenko (2004), RIMAPS and variogram characterization of water flow paths on a fracture surface, in *Dynamics of Fluids in Fractured Rock, Proceedings of the 2nd International Symposium*, edited by B. Faybishenko and P. A. Witherspoon, *Rep. LBNL-54275*, pp. 120–123, Lawrence Berkeley Natl. Lab., Berkeley, Calif.

Gallager, R. G. (1968), *Information Theory and Reliable Communication*, John Wiley, Hoboken, N. J.

Garner, D. E., J. K. Donaldson, and G. S. Taylor (1969), Entrapped soil air in a field site, *Soil Sci. Soc. Am. Proc.*, *33*, 634–635.

Gaspard, P., and R. Klages (1998), Chaotic and fractal properties of deterministic diffusion-reaction processes, *Chaos*, *8*(2), 409–423.

Gelhar, L. W. (1993), *Stochastic Subsurface Hydrology*, Prentice-Hall, Englewood Cliffs, N. J.

Geller, J. T., S. Borglin, and B. Faybishenko (2001), Water seepage in unsaturated fractures: Experiments of dripping water in fracture models and chaos analysis, *Rep. LBNL-48394*, Lawrence Berkeley Natl. Lab., Berkeley, Calif.

Gentier, S., D. Hopkins, and J. Riss (2000), Role of fracture geometry in the evolution of flow paths under stress, in *Dynamics of Fluids in Fractured Rock*, *Geophys. Monogr. Ser.*, vol. 122, edited by B. Faybishenko, P. A. Witherspoon, and S. M. Benson, pp. 169–185, AGU, Washington, D. C.

Genty, D., and G. Deflandre (1998), Drip flow variations under a stalactite of the Père Noël cave (Belgium): Evidence of seasonal variations and air pressure constraints, *J. Hydrol.*, *211*, 208–232.

Gerba, C. P., and S. M. Goyal (1985), Pathogen removal from wastewater during groundwater recharge, in *Artificial Recharge of Groundwater*, edited by T. Asano, pp. 283–317, Butterworth-Heinemann, Woburn, Mass.

Giménez, D., E. Perfect, W. J. Rawls, and Y. Pachepsky (1997), Fractal models for predicting soil hydraulic properties: A review, *Eng. Geol.*, *48*(3–4), 161–183.

Glass, R. J., and M. J. Nicholl (1996), Physics of gravity fingering of immiscible fluids within porous media—An overview of current understanding and selected complicating factors, *Geoderma*, *70*(2–4), 133–163.

Glass, R. J., J.-Y. Parlange, and T. S. Steenhuis (1989), Wetting front instability: 2. Experimental determination of relationship between system parameters and two-dimensional unstable flow field behavior in initially dry porous media, *Water Resour. Res.*, *25*(6), 1195–1207.

Glass, R. J., T. S. Steenhuis, and J. Y. Parlange (1991), Immiscible displacement in porous media: Stability analysis of three-dimensional, axisymmetric disturbances with application to gravity-driven wetting front instability, *Water Resour. Res.*, *27*(8), 1947–1956.

Glass, R. J., M. J. Nicholl, A. L. Ramirez, and W. D. Daily (2002), Liquid phase structure within an unsaturated fracture network beneath a surface infiltration event: Field experiment, *Water Resour. Res.*, *38*(10), 1199, doi:10.1029/2000WR000167.

Gleick, J. (1987), *Chaos: Making a New Science*, Viking, New York.

Grassberger, P., and I. Procaccia (1983a), Measuring the strangeness of strange attractors, *Physica D*, *9*, 189–208.

Grassberger, P., and I. Procaccia (1983b), Characterisation of strange attractors, *Phys. Rev. Lett.*, *50*, 346–349.
Haken, H. (1983), *Advanced Synergetics, Column Instability Hierarchies of Self-Organizing Systems and Devices*, Springer-Verlag, New York.
Haken, H. (1997), Visions of synergetics, *J. Franklin Inst.*, *334*(5–6), 759–792.
Hallaire, M. (1961), Irrigation et utilisation reserves naturelles, *Ann. Agron.*, *12*(1).
Harvey, R. W., and S. P. Garabedian (1991), Use of colloid filtration theory in modeling movement of bacteria through a contaminated sandy aquifer, *Environ. Sci. Technol.*, *25*, 178–185.
Hide, R. (1994), Chaos in geophysical fluids, in *Chaos and Forecasting, Proceedings of the Royal Society Discussion Meeting*, *Nonlinear Time Ser.*, vol. 2, edited by H. Tong, pp. 175–198, World Sci., River Edge, N. J.
Himasekhar, K., and H. H. Bau (1986), Large Rayleigh number convection in a horizontal, eccentric annulus containing saturated porous media, *Int. J. Heat Mass Transfer*, *29*, 703–712.
Ho, C. K. (2001), Asperity-induced episodic percolation through unsaturated fractured rock, paper presented at GSA Annual Meeting, Geol. Soc. of Am., Boston, Mass.
Horbach, J., and D. Frenkel (2001), Lattice-Boltzmann method for the simulation of transport phenomena in charged colloids, *Phys. Rev. E*, *64*, 10.1103/061507.
Indereshkumar, K., and A. L. Frenkel (1999), Wavy film flows down an inclined plane. Part I: Perturbation theory and general evolution equation for the film thickness, *Phys. Rev. E*, *60*, 4143–4157.
Jaffe, P. R., and S. W. Taylor (1993), Biomass manipulation to control pore clogging in aquifers, in *Manipulation of Groundwater Colloids for Environmental Restoration*, edited by J. F. McCarthy and F. J. Wobber, pp. 111–114, Lewis, Boca Raton, Fla.
Janosi, I. M., and V. K. Horvath (1989), Dynamics of water droplets on a window pane, *Phys. Rev. A*, *40*(9), 5232–5237.
Johns, R. A., and P. V. Roberts (1991), A solute transport model for channelized flow in a fracture, *Water Resour. Res.*, *27*(8), 1797–1808.
Kapitaniak, T. (1988), *Chaos in Systems With Noise*, World Sci., River Edge, N. J.
Kennel, M. B., R. Brown, and H. D. I. Abarbanel (1992), Determining embedding dimension for phase-space reconstruction using a geometrical construction, *Phys. Rev. A*, *45*(6), 3405–3411.
Korvin, G. (1992), *Fractal Models in the Earth Sciences*, Elsevier Sci., New York.
La Pointe, P. R. (2000), Predicting hydrology of fractured rock masses from geology, in *Dynamics of Fluids in Fractured Rock*, *Geophys. Monogr. Ser.*, vol. 122, edited by B. Faybishenko, P. A. Witherspoon, and S. M. Benson, pp. 185–202, AGU, Washington, D. C.
Lai, D., and G. Chen (1996), Dynamical systems identification from time-series data—A Hankel matrix approach, *Math. Comput. Model.*, *24*(3), 1–10.
Lai, C.-T., and G. Katul (2000), The dynamic role of root-water uptake in coupling potential to actual transpiration, *Adv. Water Resour.*, *23*, 427–439.
Lakshmi, V., and E. F. Wood (1998), Diurnal cycles of evaporation using a two-layer hydrological model, *J. Hydrol.*, *204*, 37–51.
Lenormand, R., and C. Zarcone (1989), Capillary fingering: Percolation and fractal dimension, *Transp. Porous Media*, *4*, 52–61.
Li, T. Y., and J. A. Yorke (1975), Period three implies chaos, *Am. Math. Mon.*, *82*, 985–992.
Liou, T. S. (1999), Statistical analysis of liquid seepage in partially saturated heterogeneous fracture systems, *Rep. LBNL-44823*, Lawrence Berkeley Natl. Lab., Berkeley, Calif.
Liu, H. H., C. Doughty, and G. S. Bodvarsson (1998), An active fracture model for unsaturated flow and transport in fractured rocks, *Water Resour. Res.*, *34*(10), 2633–2646.
Long, J. C. S., C. Doughty, K. Hestir, and S. Martel (1993), Modeling heterogeneous and fractured reservoirs with inverse methods based on iterated function systems, in *Reservoir Characterization III: Proceedings, Third International Reservoir Characterization Technical Conference, Tulsa, Oklahoma, November 3–5, 1991*, edited by B. Linville, pp. 471–503, Penwell, Tulsa, Okla.
Lorenz, E. N. (1963), Deterministic nonperiodic flow, *J. Atmos. Sci.*, *20*(2), 130–141.
Lorenz, E. N. (1991), Dimension of weather and climate attractors, *Nature*, *353*, 241–242.
Lorenz, E. N. (1997), *The Essence of Chaos*, Univ. of Wash. Press, Seattle.
Luthin, J. N., (Ed.) (1957), *Drainage of Agricultural Lands*, Am. Soc. of Agron., Madison, Wis.
May, R. M. (Ed.) (1981), *Theoretical Ecology: Principles and Applications*, Sinauer, Sunderland, Mass.
Meakin, P. (1991), Fractal aggregates in geophysics, *Rev. Geophys.*, *29*(3), 317–354.
Milly, P. C. D. (1996), Effects of thermal vapor diffusion on seasonal dynamics of water in the unsaturated zone, *Water Resour. Res.*, *32*(3), 509–518.
Molz, F. J., and G. K. Boman (1995), Further evidence of fractal structure in hydraulic conductivity distributions, *Geophys. Res. Lett.*, *22*(18), 2545–2548.
Molz, F. J., and H.-H. Liu (1997), Fractional Brownian motion and fractional Gaussian noise in subsurface hydrology: A review, presentation of fundamental properties, and extensions, *Water Resour. Res.*, *33*(10), 2273–2286.
Moon, F. C. (1987), *Chaotic Vibrations: An Introduction to Chaotic Dynamics for Applied Scientists and Engineers*, John Wiley, Hoboken, N. J.
Moore, M. G., A. Juel, J. M. Burgess, W. D. McCormick, and H. L. Swinney (2002), Fluctuations in viscous fingering, *Phys. Rev. E*, *65*, doi:10.1103/030601(R).
Neuman, S. P., and V. Di Federico (1998), Correlation, flow and transport in truncated multiscale permeability fields, in *Scale Dependence and Scale Invariance in Hydrology*, edited by G. Sposito, pp. 354–397, Cambridge Univ. Press, New York.
Nicholl, M. J., R. J. Glass, and S. W. Wheatcraft (1994), Gravity-driven infiltration instability in initially dry nonhorizontal fractures, *Water Resour. Res.*, *30*(9), 2533–2546.
Nicolis, C. (1987), Climatic predictability and dynamical systems, in *Irreversible Phenomena and Dynamical Systems Analysis in Geosciences*, *NATO ASI Ser., Ser. C*, vol. 192, edited by C. Nicolis and G. Nicolis, pp. 321–354, D. Reidel, Norwell, Mass.
Nicolis, G., and I. Prigogine (1989), *Exploring Complexity: An Introduction*, W. H. Freeman, New York.
Nisbet, R. M., and W. S. C. Gurney (1982), *Modeling Fluctuating Populations*, John Wiley, Hoboken, N. J.
Olsen, L. F., K. R. Valeur, T. Geest, C. W. Tidd, and W. M. Schaffer (1994), Predicting nonuniform chaotic attractors in an enzyme reaction, in *Chaos and Forecasting, Proceedings of the Royal Society Discussion Meeting*, *Nonlinear Time Ser.*, vol. 2, edited by H. Tong, pp. 161–174, World Sci., River Edge, N. J.
Or, D., and T. A. Ghezzehei (2000), Dripping into subterranean cavities from unsaturated fractures under evaporative conditions, *Water Resour. Res.*, *36*(2), 381–394.
Ortoleva, P. J. (1994), *Geochemical Self-Organization*, Oxford Univ. Press, New York.
Pachepsky, Y., and D. J. Timlin (1998), Water transport in soils as in fractal media, *J. Hydrol.*, *204*, 98–107.
Pagonabarraga, I., M. H. J. Hagen, C. P. Lowe, and D. Frenkel (1999), Short-time dynamics of colloidal suspensions in confined geometries, *Phys. Rev. E*, *59*, 4458–4469.
Pasternack, G. B. (1999), Does the river run wild? Assessing chaos in hydrological systems, *Adv. Water Resour.*, *23*(3), 253–260.
Perfect, E. (1997), Fractal models for the fragmentation of rocks and soils: A review, *Eng. Geol.*, *48*(3–4), 185–198.

Perrier, E., M. Rieu, G. Sposito, and G. de Marsily (1996), Models of the water retention curve for soils with a fractal pore size distribution, *Water Resour. Res.*, *32*, 3025–3032.

Persoff, P., and K. Pruess (1995), Two-phase flow visualization and relative permeability measurement in natural rough-walled rock fractures, *Water Resour. Res.*, *31*(5), 1175–1186.

Plourde, B. N., and M. Bretz (1993), Water droplet avalanches, *Phys. Rev. Lett.*, *71*, 2749–2752.

Podgorney, R., T. Wood, B. Faybishenko, and T. Stoops (2000), Spatial and temporal instabilities in water flow through variably saturated fractured basalt on a one-meter scale, in *Dynamics of Fluids in Fractured Rock*, *Geophys. Monogr. Ser.*, vol. 122, edited by B. Faybishenko, P. A. Witherspoon, and S. M. Benson, pp. 129–146, AGU, Washington, D. C.

Prazak, J., M. Sir, F. Kubik, J. Tywoniak, and C. Zarcone (1992), Oscillation phenomena in gravity-driven drainage in coarse porous media, *Water Resour. Res.*, *28*(7), 1849–1855.

Priest, S. D. (1993), *Discontinuity Analysis for Rock Engineering*, Chapman and Hall, New York.

Prigogine, I., and I. Stengers (1997), *The End of Certainty: Time, Chaos, and the New Laws of Nature*, Free Press, New York.

Pruess, K. (1999), A mechanistic model for water seepage through thick unsaturated zones in fractured rocks of low matrix permeability, *Water Resour. Res.*, *35*(4), 1039–1052.

Pruess, K. (2000), Multiphase flow in fractured rocks—Some lessons learned from mathematical models, in *Dynamics of Fluids in Fractured Rock*, *Geophys. Monogr. Ser.*, vol. 122, edited by B. Faybishenko, P. A. Witherspoon, and S. M. Benson, pp. 225–234, AGU, Washington, D. C.

Pruess, K., B. Faybishenko, and G. S. Bodvarsson (1999), Alternative concepts and approaches for modeling flow and transport in thick unsaturated zones of fractured rocks, *J. Contam. Hydrol.*, *38*, 281–322.

Pyrak-Nolte, L., L. R. Myer, and D. D. Nolte (1992), Fractures: Multifractals and finite-size scaling, *Pure Appl. Geophys.*, *138*(4), 679–706.

Pyrak-Nolte, L. J., D. D. Nolte, and N. G. W. Cook (1995), Hierarchical cascades and the single fracture: Percolation and seismic detection, in *Fractals in Petroleum Geology and Earth Processes*, edited by C. C. Barton and P. R. La Pointe, pp. 143–178, Plenum, New York.

Rabinovich, M. I., and D. I. Trubetskov (1994), *Oscillations and Waves in Linear and Nonlinear Systems*, Kluwer Acad., Norwell, Mass.

Rabinovich, M. I., A. B. Ezersky, and P. D. Weidman (2000), *The Dynamics of Patterns*, World Sci., River Edge, N. J.

Read, P. L. (2001), Editorial, *Nonlinear Processes Geophys.*, *8*, 191–192.

Renard, F., and P. Ortoleva (1997), Water films at grain-grain contacts—Debye-Huckel, osmotic model of stress, salinity, and mineralogy dependence, *Geochim. Cosmochim. Acta*, *61*(10), 1963–1970.

Renard, F., J. P. Gratier, P. Ortoleva, E. Brosse, and B. Bazin (1998), Self-organization during reactive fluid flow in a porous media, *Geophys. Res. Lett.*, *25*(3), 385–388.

Renshaw, C. E. (2000), Fracture spatial density and the anisotropic connectivity of fracture networks, in *Dynamics of Fluids in Fractured Rock*, *Geophys. Monogr. Ser.*, vol. 122, edited by B. Faybishenko, P. A. Witherspoon, and S. M. Benson, pp. 203–211, AGU, Washington, D. C.

Rieu, M., and G. Sposito (1991), Fractal fragmentation, soil porosity, and soil water properties: II. Applications, *Soil Sci. Soc. Am. J.*, *55*, 1239–1244.

Ritsema, C. J., L. W. Dekker, J. L. Nieber, and T. S. Steenhuis (1998), Modeling and field evidence of finger formation and finger recurrence in a water repellent sandy soil, *Water Resour. Res.*, *34*(4), 555–567.

Rittman, B. E. (1993), The significance of biofilms in porous media, *Water Resour. Res.*, *29*(7), 2195–2202.

Rodriguez-Iturbe, I., D. Entekhabi, and R. L. Bras (1991), Nonlinear dynamics of soil moisture at climate scales: 1. Stochastic analysis, *Water Resour. Res.*, *27*(8), 1899–1906.

Rodriguez-Iturbe, I., D. Entekhabi, J. S. Lee, and R. L. Bras (1991), Nonlinear dynamics of soil moisture at climate scales: 2. Chaotic analysis, *Water Resour. Res.*, *27*(8), 1907–1915.

Rosendahl, J., M. Vekic, and J. Kelley (1993), Persistent self-organization of sandpiles, *Phys. Rev. E*, *47*, 1401–1447.

Sahimi, M. (1993), Flow, dispersion, and displacement processes in porous media and fractured rocks: From continuum models to fractals, percolation, cellular automata and simulated annealing, *Rev. Mod. Phys.*, *65*(4), 1393–1534.

Salve, R., and C. M. Oldenburg (2001), Water flow in a fault in altered nonwelded tuff, *Water Resour. Res.*, *37*(12), 3043–3056.

Salve, R., J. S. Y. Wang, and C. Doughty (2002), Liquid release tests in unsaturated fractured welded tuffs: I. Field investigations, *J. Hydrol.*, *256*, 60–79.

Schuster, H. G. (1988), *Deterministic Chaos: An Introduction*, 2nd rev. ed., John Wiley, Hoboken, N. J.

Selker, J. S., T. S. Steenhuis, and J. Y. Parlange (1992), Wetting-front instability in homogeneous sandy soils under continuous infiltration, *Soil Sci. Soc. Am. J.*, *56*(5), 1346–1350.

Shannon, C. E., and W. Weaver (1949), *The Mathematical Theory of Communication*, Univ. of Ill. Press, Urbana.

Shaw, R. (1984), *The Dripping Faucet as a Model Chaotic System*, Aerial, Santa Cruz, Calif.

Sililo, O. T. N., and J. H. Tellam (2000), Fingering in unsaturated zone flow: A qualitative review with laboratory experiments on heterogeneous systems, *Groundwater*, *38*(6), 864–871.

Sivashinsky, G. I., and D. M. Michelson (1980), *Prog. Theor. Phys.*, *63*, 2112–2114.

Sparrow, C. (1982), *The Lorenz Equations, Bifurcations, Chaos, and Strange Attractors*, Springer-Verlag, New York.

Sposito, G. (1994), Steady groundwater flow as a dynamical system, *Water Resour. Res.*, *30*(8), 2395–2401.

Sprott, J. C., and G. Rowlands (1995), Chaos data analyzer: The professional version (2.1), software, Phys. Acad. Software, Raleigh, N. C.

Stothoff, S., and D. A. Or (2000), Discrete-fracture boundary integral approach to simulating coupled energy and moisture transport in a fractured porous medium, in *Dynamics of Fluids in Fractured Rock*, *Geophys. Monogr. Ser.*, vol. 122, edited by B. Faybishenko, P. A. Witherspoon, and S. M. Benson, pp. 267–279, AGU, Washington, D. C.

Su, G. W., J. T. Geller, K. Pruess, and F. Wen (1999), Experimental studies of water seepage and intermittent flow in unsaturated, rough-walled fractures, *Water Resour. Res.*, *35*(4), 1019–1037.

Swinney, H. L., and J. P. Gollub (Eds.) (1985), *Hydrodynamic Instabilities and the Transition to Turbulence*, 2nd ed., Springer-Verlag, New York.

Timmer, J., S. Haussler, M. Lauk, and C.-H. Lucking (2000), Pathological tremors: Deterministic chaos or nonlinear stochastic oscillators?, *Chaos*, *10*(1), 278–288.

Tokunaga, T. K., and J. Wan (1997), Water film flow along fracture surfaces of porous rock, *Water Resour. Res.*, *33*(6), 1287–1295.

TruSoft International, Inc. (1997), Benoit Software™, St. Petersburg, Fla.

Tsang, Y. (1984), The effect of tortuosity on fluid flow through a single fracture, *Water Resour. Res.*, *20*(9), 1209–1215.

Tsonis, A. A. (1992), *Chaos: From Theory to Applications*, Plenum, New York.

Turcotte, D. L. (1997), *Fractals and Chaos in Geology and Geophysics*, Cambridge Univ. Press, New York.

Turing, A. M. (1952), The chemical basis of morphogenesis, *Philos. Trans. R. Soc. London, Ser. B*, *237*, 37–72.

Tyler, S. W., and S. W. Wheatcraft (1990), The consequences of fractal scaling in heterogeneous soils and porous media, in *Scaling in Soil Physics: Principles and Applications*, edited by D. Hillel and E. Elrick, *SSSA Spec. Publ.*, *25*, 109–122.

2089 Unger, A. J. A., B. Faybishenko, G. S. Bodvarsson, and A. M.
2090 Simmons (2004), Simulating infiltration tests in fractured basalt
2091 at the Box Canyon site, Idaho, *Vadose Zone J.*, *3*, 75–89.
2092 Vandevivere, P., P. Baveye, D. Sanchez de Lozada, and P. DeLeo
2093 (1995), Microbial clogging of saturated soils and aquifer materi-
2094 als: Evaluation of mathematical models, *Water Resour. Res.*,
2095 *31*(9), 2173–2180.
2096 Walmann, T., A. Malthe-Sørenssen, J. Feder, T. Jøssang, P. Meakin,
2097 and H. H. Hardy (1996), Scaling relations for the lengths and
2098 widths of fractures, *Phys. Rev. Lett.*, *77*, 5393–5396.
2099 Wang, Z., J. Feyen, M. T. van Genuchten, and D. R. Nielsen
2100 (1998), Air entrapment effects on infiltration rate and flow in-
2101 stability, *Water Resour. Res.*, *34*(2), 213–222.
2102 Weeks, S. W., and G. Sposito (1998), Mixing and stretching effi-
2103 ciency in steady and unsteady groundwater flows, *Water Resour.*
2104 *Res.*, *34*(12), 3315–3322.
2105 Wheatcraft, S. W., and J. H. Cushman (1991), Hierarchical
2106 approaches to transport in porous media, *U.S. Natl. Rep. Int. Un-*
2107 *ion Geod. Geophys. 1987–1990*, *Rev. Geophys.*, *29*, 263–269.
2108 Williams, G. P. (1997), *Chaos Theory Tamed*, Joseph Henry,
2109 Washington, D. C.
Witherspoon, P. A., J. S. W. Wang, K. Iwai, and J. E. Gale (1980), 2110
Validity of cubic law for fluid flow in a deformable rock fracture, 2111
Water Resour. Res., *16*(6), 1016–1024. 2112
Yao, Q., and H. Tong (1994), On prediction and chaos in stochastic 2113
systems, in *Chaos and Forecasting, Proceedings of the Royal* 2114
Society Discussion Meeting, *Nonlinear Time Ser.*, vol. 2, edited 2115
by H. Tong, pp. 57–86, World Sci., River Edge, N. J. 2116
Yortsos, Y. (2000), Physical considerations in the upscaling of 2117
immiscible displacements in a fractured medium, in *Dynamics* 2118
of Fluids in Fractured Rock, *Geophys. Monogr. Ser.*, vol. 122, 2119
edited by B. Faybishenko, P. A. Witherspoon, and S. M. Benson, 2120
pp. 235–249, AGU, Washington, D. C. 2121
Yu, L. Q., F. K. Wasden, A. E. Dukler, and V. Balakotaian (1995), 2122
Nonlinear evolution of waves on falling films at high Reynolds 2123
numbers, *Phys. Fluids*, *7*(8), 1886–1902. 2124

B. Faybishenko, Earth Sciences Division, Ernest Orlando Lawrence 2126
Berkeley National Laboratory, 1 Cyclotron Road, Library Building 50B, 2127
Berkeley, CA 94720, USA. (bfayb@llbl.gov) 2128